IMPERIAL COLLEGE OF SCIENCE AND TECHNOLOGY

Fluids Section, Mechanical Engineering Department

Exhibition Road, London SW7 2BX

Flow in out-of-plane double S-bends

by

M.C. Schmidt, J.H. Whitelaw and M. Yianneskis[+]

[+]King's College London
Mechanical Engineering Department
Strand, London WC2R 2LS

prepared for

June 1986   FS/86/30

ABSTRACT

Developing flows in two out-of-plane double S-bend configurations have been measured by laser-Doppler anemometry. The first duct had a rectangular cross-section 40mmx40mm at the inlet and consisted of a uniform area 22.5°-22.5° S-duct upstream with a 22.5°-22.5° S-diffuser downstream. The second duct had a circular cross-section and consisted of a 45°-45° uniform area S-duct upstream with a 22.5°-22.5° S-diffuser downstream. In both configurations the ratio of the mean radius of curvature to the inlet hydraulic diameter was 7.0, the exit-to-inlet area ratio of the diffusers was 1.5 and the ducts were connected so that the centerline of the S-duct lay in a plane normal to that of the S-diffuser.

Streamwise and cross-stream velocity components were measured in laminar flow for the rectangular duct and in turbulent flow for both configurations; measurements of the turbulence levels, cross-correlations and wall static pressures were also made in the turbulent flow cases. Secondary flows of the first kind are present in the first S-duct and they are complemented or counteracted by the secondary flows generated by the area expansion and by the curvature of the S-diffusers downstream. Cross-stream velocities with magnitudes up to 0.19 and 0.11 of the bulk velocity were measured in the laminar and turbulent flows respectively in the rectangular duct and six cross-flow vortices were evident at the exit of the duct in both flow cases. The turbulent flow in the circular duct was qualitatively similar to that in the rectangular configuration, but the cross-stream velocities measured at the exit plane were smaller in the circular geometry.

The results are presented in sufficient detail and accuracy for the assessment of numerical calculation methods and are listed in tabular form for this purpose.

KEYWORDS

Ducts – Intake systems

Subsonic diffusers

Curved diffusers

TABLE OF CONTENTS

SUMMARY

An experimental investigation of developing flows through two out-of-plane double S-bend ducts is presented. Measurements were made in a duct of rectangular cross-section at Reynolds numbers of 790 and 40,000, and in a duct of circular cross-section at a Reynolds number of 48,000. Laser-Doppler anemometry was used to measure the velocity components and, in the turbulent flow cases, the turbulence levels and cross-correlations. Wall static pressure measurements are also presented for the turbulent flow cases in both ducts. In both ducts the centreline of the second S-bend lay in a plane normal to that of the first S-bend, and the ratio of the mean radius of curvature to the hydraulic diameter at the duct inlet was 7.0. The rectangular duct consisted of a constant area $22.5°-22.5°$ S-duct upstream connected to a $22.5°-22.5°$ S-diffuser of 1.5 exit-to-inlet area ratio downstream. The circular duct consisted of a constant area $45°-45°$ S-duct upstream with a $22.5°-22.5°$ S-diffuser of 1.5 area ratio downstream. The boundary layers at the duct inlets were approximately 25% and 15% of the hydraulic diameter in the laminar and turbulent flows respectively.

Pressure-driven secondary flows were generated in each of the four constituent bends in both flow configurations. The cross-flows were larger in the laminar flow case, due partly to the difference in the inlet boundary layer thicknesses. The maximum cross-flow velocities measured at the exit plane were 0.19 and 0.11 of the bulk velocity, V_B, for the laminar and turbulent flows in the rectangular duct, and 0.03 V_B for the flow measurements made in the circular duct. In all flow cases, the secondary flows generated in the first S-bend had a strong influence on the flow patterns in the second S-bend. The velocity and turbulence quantity distributions at the exit plane of the second S-bends show similarities to the patterns observed in single S-bend configurations, but the patterns are asymmetric with up to six cross-flow vortices present. The recovery of the flows in the downstream tangent is very gradual, especially in the laminar case.

The results have been obtained and are presented in detail and are of benchmark accuracy so that they can be used for the evaluation of numerical methods for the calculation of the flows. Accordingly, the measurements are listed in tabular form.

1. INTRODUCTION

Flow configurations where a combination of out-of-plane bends are employed are encountered in practice in aircraft wing-root intakes, and the efficient re-direction of the flow, with some pressure recovery and a uniform velocity profile at the duct exit (i.e. at the turbine compressor face) are normal requirements. There are a number of problems associated with the design of the intakes as the intake geometry must accomodate the constraints imposed by the location, shape and size of the propulsion turbine and of the fuselage. In order to reduce the likelihood of flow separation at the walls of the ducts, small centreline displacement and relatively mild curvature ducts are used. The flows in these intake passages are developing and three-dimensional, with thin inlet boundary layers.

Investigations of the flow in constant area single S-ducts have been reported in reference 1 for square cross-section ducts and in references 2 and 3 for circular cross-section ducts. Pressure-driven secondary flows were generated in the first bend and a similar cross-flow, but in the opposite direction, was established in the second bend; however, at the exit of the S-ducts the secondary flow generated in the first bend was partly sustained due to the local sign of the radial vorticity. References 4 and 5 reported measurements of laminar and turbulent developing flows through S-shaped diffusers of 1.5 exit-to-inlet area ratio in rectangular and circular cross-section ducts respectively. The cross-stream flows in the S-diffusers result from both the curvature-induced secondary motion and from the increase in area; the measured maximum of the radial velocity was 0.4 of the bulk velocity, V_B, in the laminar flow case and 0.1-0.15V_B in the turbulent flow cases. In both constant area and diffusing ducts larger secondary flows were measured in the laminar flow cases, due partly to the thicker inlet boundary layers encountered at the lower Reynolds numbers. The influence of the inlet conditions on the incipient separation in the flows in C-shaped 45° diffusers was examined in reference 6. Numerical calculations of the flows in S-ducts have been reported in references 7-10. In the absence of large regions of flow separation, finite-difference forms of the Navier-Stokes equations were solved by forward-marching procedures with considerable savings in computational storage and time. Qualitative (reference 8) and quantitative (references 7, 9 and 10) comparisons with experimental data have shown good agreement.

The present configurations were based on the dimensions of the single S-ducts and S-diffusers of references 1, 3, 4 and 5 in order to enable comparisons to be made with ducts of simpler geometry and to aid the understanding of the flow processes and the interpretation of the data.

Left- and right-hand-side out-of-plane double S-bend intake geometries are mirror images of each other about a vertical plane which contains the aircraft axis. Assuming that the symmetry plane of the first S-bend is horizontal and that of the second S-bend vertical, the bend curvature and the direction of the secondary flows at the exit of the first S-bend on the right hand side will be in the opposite sense to that at the corresponding plane on the left hand side duct. The bend curvature and secondary flows generated in either of the second S-bends will be identical in direction. Therefore the superimposition of the secondary flows generated in the first S-bend (different in the right and in the left intakes) onto those

2

generated in the second S-bend (identical in both intakes), will result in a different cross-flow pattern at the turbine compressor face from each intake duct. The right- and left-hand-side intake flow patterns should be expected to be mirror images of each other. In the present investigation left-hand-side intakes were investigated, but extrapolation to right-hand intakes can be made.

The flow configuration and experimental techniques are described in the following section. The results are presented and discussed in section 3, and a summary of the main findings is given in section 4.

2. FLOW CONFIGURATION AND EXPERIMENTAL TECHNIQUES

2.1 Flow Configurations

The flow configurations and coordinate systems are shown in Figures 1 and 2. Both configurations consisted of a combination of a uniform cross-sectional area S-duct upstream connected in series to a 1.5 exit-to-inlet area ratio S-diffuser downstream. The inlet and exit planes were parallel in both configurations, and the centreline of the diffusing duct lay in a plane normal to that containing the centreline of the first duct. The rectangular duct configuration consisted of a square cross-section (40mmx40mm) 22.5°-22.5° S-bend upstream and a rectangular cross-section 22.5°-22.5° S-diffuser downstream. The circular duct configuration consisted of a 45°-45° constant cross-sectional area S-duct of 48mm diameter upstream with a 22.5°-22.5° S-diffuser downstream. The increase in the cross-sectional area of the diffusers was made in a linear fashion, so that the area of any cross-section was proportional to its centerline distance from the beginning of the area expansion. The radius ratio, i.e. the ratio of the radius of curvature of the centreline (R_c, 280mm for the rectangular duct, and 336mm for the circular duct) to the hydraulic diameter at the duct inlet (D, 40mm for the rectangular duct and 48mm for the circular duct) was 7.0 for both ducts. The rectangular S-diffuser expanded in area to a rectangular outlet 40mmx60mm so that only the radial dimension changed while the spanwise dimension was kept constant along the length of the duct. The effective total divergence angle, for a straight diffuser equivalent to the present curved ones, was 2.4 and 5.2 degrees for the circular and rectangular diffusers respectively. The lengths of the upstream and downstream tangents and of the spacer are shown in Figures 1(a) and 2. The upstream tangents were preceded by smooth area contractions with honeycomb screens and in the rectangular duct case by a 0.5mm boundary layer trip. The water tunnels were identical to those described in detail in references 4 and 5. The flow rates were kept constant by precision bore flowmeters.

For consistency of presentation, the coordinate notation at the inlet is kept unaltered through the double S-bends, i.e. there was no rotation of r^* and z^* directions upon entry to the out-of-plane second S-bend, even though as a result of this coordinate notation the plane of curvature of the second bend is not the radial coordinate plane as normally defined in previous investigations. The z^* direction lies always in a vertical plane and the r^* direction lies in a horizontal plane throughout the duct length. However, in order to enable comparisons with previous investigations in single S-bends, the notation of the cross-stream velocity components in

the second bend was made so that components in the plane of curvature (in the z* direction) are denoted V,V and v and the components in the spanwise (r*) direction are denoted W,W and w (see Figure 1(b)), in direct correspondence with the notation used in references 1, 3, 4 and 5. The streamwise distance (X) is measured in hydraulic diameters along the centerline from the inlet of the first S-bend; in addition, and in order to enable direct comparison of the flow development with that in single S-diffusers, the coordinate X* was measured in hydraulic diameters (D) from the inlet of the present S-diffusers.

Measurements were made at Reynolds numbers, based on the hydraulic diameter and bulk velocity at the upstream tangent, of 790 and 40,000 in the rectangular duct and 48,000 in the circular duct. The bulk velocities (V_B) were 1.00m/s for both turbulent flows (i.e. for Re=40,000 and 48,000) and 19.75mm/s in the laminar flow case in the rectangular duct.The corresponding Dean numbers are 10,690, 12,828 and 212. Water was employed as the fluid medium to obtain the same Reynolds number at a scale much smaller than that achieved in air.

2.2 Laser-Doppler Velocimeter, Experimental Procedure and Accuracy

The laser-Doppler anemometer was of the dual-beam type and operated in forward scatter, and made use of a 5mW HeNe laser, a diffraction grating and associated optics and a frequency tracker demodulator for the processing of the Doppler signals. The grating was used to split and frequency shift the beams. The principal characteristics of the optical system are given below in Table I. The flows were seeded with small quantities of milk (about 20ml in 10,000 litres) in order to increase the scattering particle concentration.

Measurements in the rectangular diffuser were made with the beams oriented in three directions (0, 45 and -45 degrees to the local streamwise direction) in the X-r* plane in the S-duct (and downstream of the S-diffuser for the $\overline{W}$, $\tilde{w}$ and $\overline{uw}$ component measurements) and in the X-z* plane in the S-diffuser with the beams entering the test section through the flat side-walls in both cases. The Doppler frequencies measured were resolved to provide the local streamwise (U,$\overline{U}$ and $\tilde{u}$) and and cross-stream (V, $\overline{V}$ and $\tilde{v}$ and $\overline{W}$ and $\tilde{w}$) components and the corresponding cross-correlations ($\overline{uv}$ and $\overline{uw}$ respectively).

The circular duct had flat external surfaces to minimise beam refraction at the air/Plexiglass interface, and measurements were made in the manner described in reference 3. The streamwise component was obtained with the beams on an X-r* plane entering the duct through the r*=0.0 side and the radial components with the beams on a r*-z* plane entering through the r*=0.0 side of the duct. The refraction correction analyses for the location of the measuring volume and for the anemometer transfer constant are given in reference 3.

The instrumentation and experimental techniques have been described in detail in reference 11, and estimates of the tolerances in the measured quantities are listed in Table II below. As the measurement procedures for the rectangular and for the circular ducts were different, the error estimates shown in Table II are also different for the two flow

4

configurations. In brief, the measurement errors are of the order of 1% rising to 2-3% in regions of steep gradients. Measurements were made at both sides of the symmetry plane at the inlets of all ducts and confirmed symmetry within the measurement precision in all flow cases.

Wall static pressures were measured, through tappings let into the walls of the ducts, by a differential micromanometer. Measurements were made for the turbulent flow cases only, as the pressure differences in laminar flow were within the precision of the micromanometer.

Table I Principal characteristics of the laser anemometer optical system

Half-angle of beam intersection in air (degrees)	9.35
Frequency-to-velocity transfer constant (m/s/MHz)	1.947
Intersection volume diameter at $1/e^2$ intensity (μm)	200
Intersection volume length at $1/e^2$ intensity (μm)	1560
Number of fringes in intersection volume without shifting	100
Fringe separation (line-pair spacing) (μm)	1.947

Table II Maximum estimates of measurement errors

Quantity	Systematic error	Random error
X, X*	0.5mm	±0.02mm
r*, z*	0.5mm	±0.02mm
V_B (laminar)	1%	±1%
V_B (turbulent)	nil	±0.75%
Frequency shift	less than 1%	±0.5%
C_p	less than 1%	±1.7%

Rectangular duct

Quantity	Systematic error	Random error
U	up to 2.5%	±1%
V	up to 3%	±1.5%
W	up to 3%	±1.5%
$\tilde{u}$	up to 3%	up to 3%
$\tilde{v}$	up to 3%	up to 5%
$\tilde{w}$	up to 3%	up to 5%
$\overline{uv}$	1.5%	±2.5% to ±8.5%
$\overline{uw}$	1.5%	±2.5% to ±8.5%

Circular duct

Quantity	Systematic error	Random error
U	up to 2%	±1%
V	up to 4%	±1%
$\tilde{u}$	up to 2%	up to 3%
$\tilde{v}$	up to 2%	up to 3%

N.b. There is no systematic error in V_B (turbulent) because the flowmeter has been independently calibrated.

Percentage errors refer to errors in local value.

6

3. RESULTS

Measurements made in the first S-bend in both configurations showed that the inlet conditions were identical to those in the single, uniform-area S-ducts of references 1 and 3, and that the second S-bend had an influence on the flow up to about two hydraulic diameters upstream of the inlet of the diffuser. As a result, the measurement programme presented here concentrated on the characteristics of the flows in the second S-bend and especially at the duct exit.

3.1 Rectangular cross-section duct - Laminar flow

Figure 3 shows the variation of the streamwise (U) velocity component along the centerline of the S-diffuser. It rises sharply from $0.95V_B$ at the diffuser inlet to around $1.5V_B$ at 3.8 D downstream of the inlet and subsequently decreases to around $1.4V_B$ at the diffuser exit.

The centreline distribution of the radial component of velocity through the diffuser is shown in Figure 4. There are two reversals of the sign of the velocity which decreases from $0.03V_B$ at the inlet to $-0.155V_B$ at around 2.8D and thereafter increases sharply to reach a value of $0.156V_B$ at the diffuser exit.

The streamwise velocity profiles at the exit plane of the S-diffuser are shown in Figure 5 for $r^*=0.1-0.9$ and the corresponding V velocity profiles are shown in Figure 6. The U velocity profiles show an asymmetric flow pattern at the exit with two peaks evident in all but the $r^*=0.1$ profile. The four $\delta U/\delta r$ gradients associated with the two peaks indicate the existence of secondary flow cells like those encountered at the exits of bends with symmetric inlet conditions (see e.g. reference 12) but of dissimilar magnitude. The small peak near $z^*=-1.0$, $r^*=0.7$ indicates the existence of another cross-flow motion in that region.

The V velocity profiles at the duct exit (Figure 6) indicate a complex cross-flow pattern with a predominant direction towards the $z^*=-1.0$ wall, i.e. the outer wall with respect to the center of curvature at the exit of the diffuser. There are four regions of negative V velocity (i.e. directed towards the $z^*=1.0$ wall), two at $r^*=0.1$, around $z^*=-0.6$ and 0.9, and two at $r^*=0.9$, around $z^*=0.1$ and 0.8. The results show six cross-flow motions, one in each corner of the duct and two around $z^*=0.1$, $r^*=0.9$. Three of the vortices rotate in a counter-clockwise direction and three in a clockwise fashion (viewing the exit plane as in Figure 1(b)). There is some evidence of the cross-flow indicated by the U results near the wall at $r^*=0.7$ by the local peak in V, but no local negative values of V were recorded; it should expected though that closer to the wall, where measurements were not possible due to optical access limitations, negative V velocities will be present.

Measurements were made in the downstream tangent to examine the recovery of the flow downstream of the double S-bend. Streamwise (U) and cross-stream (V) velocity profiles at $r^*=0.5$, $X^*=12.375$ and 16.735 (6.875 and 10.875D downstream of the exit of the diffuser) are shown in Figures 7(a)-(d). The U velocity profiles show that the recovery of the flow is very slow and at the further downstream station (Fig. 7(b)) the large

gradients in the profile indicate the persistently strong influence of the S-bends located upstream. The V velocity profiles show that cross-flows, with maxima of 0.105 and 0.07 V_B respectively at the two stations, are still in evidence. It can be reasonably expected that the flow does not recover fully until far downstream in the tangent.

The measurements are tabulated in Appendix 1 as Table 1.1.

3.2 Rectangular cross-section duct - Turbulent flow

The wall static pressure measurements are presented in Figure 8 as plots of the variation of the pressure coefficient, $C_P=(P-P_{ref})/\frac{1}{2}\rho V_B^2$, with streamwise distance. Four variations of C_P with X^* are shown: along the $r^*=0.0$ wall at $z^*=0.0$, along the $z^*=-1.0$ wall at $r^*=0.5$, along the $r^*=1.0$ wall at $z^*=0.0$, and along the $z^*=1.0$ wall at $r^*=0.5$. The pressure gradients set up by each bend can be distinguished and are separated very near the inflexion point in the middle of each of the S-bends and near the middle of the spacer between the two S-bends. The radial pressure gradients in each of the four constituent bends have maxima of approximately 0.25, 0.26, 0.27 and 0.17 of $\frac{1}{2}\rho V_B^2$ respectively. The pressure drop through the S-duct is around 0.15 of the velocity head (ρV_B^2) and the pressure recovery through the S-diffuser is around $0.21\rho V_B^2$: there is thus an overall pressure rise of about one twentieth of the velocity head across the whole duct.

The variation of the mean velocity component along the centreline of the S-diffuser is shown in Figure 9. The $\bar{U}$ velocity decreases from a value of $1.2V_B$ at the inlet to around $0.93V_B$ at the diffuser exit. The corresponding centreline variation of the radial $(\bar{V})$ mean velocity component is shown in Figure 10. There are two changes in the sign of $\bar{V}$ and the variation follows closely the trend observed in the laminar flow case. The magnitudes of $\bar{V}$ decrease from $0.06V_B$ at the inlet of the diffuser to $-0.16V_B$ around $X^*=2.8$ and rise again to a value of $0.06V_B$ at the exit plane.

The centreline variations of the $\tilde{u}$ and $\tilde{v}$ turbulence levels and of the $\overline{uv}$ cross-correlations are shown in Figures 11, 12 and 13 respectively. The $\tilde{u}$ levels rise from $0.015V_B$ at the diffuser inlet to $0.065V_B$ at the exit. Similarly, the $\tilde{v}$ levels increase through the diffuser from 0.008 at the inlet to 0.042 V_B at the exit. The cross-correlations have expectedly very small values along the duct centreline until $X^*=4.0$ and rise to a maximum value of $0.0008V_B^2$ in the vicinity of the diffuser exit where there is strong cross-flow activity. The scatter near $X^*=3.0$ in Fig.13 is due to the extremely small magnitudes of $\overline{uv}$, which are within the experimental precision in the region up to $X^*=4.0$.

Streamwise mean velocity profiles measured at $r^*=0.1$, 0.3, 0.5, 0.7 and 0.9 at three axial stations and at $r^*=0.3$ and 0.7 at one axial station in the duct are shown in Figures 14 to 17. The measurements in station 1 -at the inlet of the S-duct- are presented in Figure 14 and can be compared with those reported in the uniform-area single S-duct investigation of reference 1. There is excellent agreement between the two data sets indicating that there is no upstream influence of the second S-bend at this station. The profiles at station 2 (Figure 15), at the exit of the first S-bend, are however slightly asymmetric, indicating a small influence of the second S-bend. The asymmetry in the profiles at the inlet of the second S-

8

bend is also small (Fig.16), but large asymmetries are evident in all profiles at the exit plane of the diffuser (Figure 17). The $r^*=0.1$, 0.3 and 0.5 profiles at the exit plane have only one peak, but those at $r^*=0.7$ and 0.9 have two maxima and show qualitative similarities with the laminar U profiles presented in the previous section, but the peaks are less pronounced in the turbulent flow case and the near-wall velocity magnitudes are larger. The latter result indicates that the thicknesses of the boundary layers on all four walls of the duct are smaller than for laminar flow. The results indicate that the low-turbulence near-potential core flow is located near $r^*=0.4$, and that two secondary flow cells are present near the $r^*=1.0$ wall.

The corresponding radial mean velocity profiles at the exit plane are presented in Figure 18. The maximum $\overline{V}$ velocity measured was $0.11V_B$ at $r^*=0.7$ and the cross-flow direction was towards the $z^*=-1.0$ wall except for two small regions at the two corners of the duct near the $z^*=1.0$ wall, where negative $\overline{V}$ velocities of up to $0.04 V_B$ were measured. In comparison with the laminar flow results, the measured cross-stream velocity magnitudes are smaller in turbulent flow. The presence of two counter-rotating cross-flow vortices, which correspond to the secondary flows generated at the second bend of the S-diffuser, is shown by the $\overline{V}$ measurements.

Locating screws prohibited the measurement of the spanwise $(\overline{W})$ velocities at the exit of the S-diffuser, and measurements of the $\overline{W}$, $\tilde{w}$ and $\overline{uw}$ components were made at a station 13mm (0.325D) downstream of the exit, i,e, at $X^*=5.825$. The $\overline{W}$ results at this station can be reasonably expected to be quantitatively similar to the patterns at the duct exit plane. The spanwise mean velocity measurements are presented in Figure 19 and suggest six cross-flow vortices, as in the laminar flow case, with measured maxima of around $0.05V_B$.

The mean flow results show the existence of a very complex flow pattern at the duct exit. Consideration of all three velocity component measurements (Figures 17, 18 and 19) indicates that there are six cross-stream vortices in the r^*-z^* plane at the duct exit, four located around $r^*=0.7$ and two around $r^*=0.3$.

The streamwise turbulence levels at the duct exit (Figure 20) have nearly uniform distributions near the two side walls with magnitudes around $0.068V_B$, while in the remainder of the cross-section the levels vary from 0.11 down to 0.03 V_B. The radial turbulence levels (Figure 21) have smaller magnitudes with measured maxima of around $0.06V_B$, but exhibit qualitatively similar distributions to the u results. The scatter in the v profiles is of the order of $0.01V_B$, within the experimental error quoted which is larger than that for $\tilde{u}$ as three separate measurements must be made to resolve $\tilde{v}$, in comparison with one for $\tilde{u}$ and two for $\overline{uv}$. The $\overline{uv}$ cross-correlations are presented in Figure 22 and have maxima of around $0.0032V_B{}^2$. The $\tilde{w}$ levels measured at 0.325D downstream of the exit (Figure 23) do not exceed $0.056V_B$. The corresponding $\overline{uw}$ cross-correlations shown in Figure 24 have maximum magnitudes approximately two-thirds those of the $\overline{uv}$ ones.

The development of the flow in the downstream tangent is indicated by the results of Figure 25(a) and (b). Profiles of streamwise and radial mean

velocity at $r^*=0.5$, at 6.875 and 10.875D downstream of the diffuser exit are shown and can be compared with the corresponding laminar flow results. The profiles of both velocity components are more uniform than in laminar flow, and show that the flow recovery is more rapid in the turbulent case. The maximum $\overline{V}$ velocity decreases from $0.047V_B$ in the upstream to $0.042V_B$ in the downstream station.

The results are listed in Table 1.2 in Appendix 1.

3.3 Circular cross-section duct

Measurements were made in the circular duct at a Reynolds number of 48,000 and with the same bulk velocity (1.00 m/s) through the duct as for the results of section 3.2.

The centerline variation of the streamwise mean velocity through the circular cross-section S-diffuser is shown in Figure 26. The $\overline{U}$ values measured decrease, as the cross-sectional area increases, from $0.96V_B$ at the inlet to $0.82V_B$ at the exit of the diffuser. Measurements of the centerline variation of $\overline{V}$ are shown in Figure 27. $\overline{V}$ decreases from $0.02V_B$ at the inlet to $-0.05V_B$ at $X^*=2.9$ and subsequently increases to $0.015V_B$ at the exit. The $\tilde{u}$ and $\tilde{v}$ turbulence levels along the centerline (Figures 28 and 29) have maxima of 0.053 and $0.044V_B$ respectively and are nearly constant throughout the length of the diffuser, in contrast to the marked increase found in the rectangular duct. This difference in the centerline development of the turbulence levels is a result of the different migration of the near-potential "core" flow region through the ducts in the two geometries.

The contours of the streamwise mean velocity at the duct exit plane are shown in Figure 30. The maximum and minimum $\overline{U}$ velocities measured were 0.86 and $0.42V_B$ respectively. The streamwise turbulence level contours at the duct exit are presented in Figure 31. The measured maximum of $\tilde{u}$ was $0.097V_B$, located around $z^*=-0.4$ and $r^*=0.6$.

Profiles of the radial mean and r.m.s. velocity components ($\overline{V}$ and $\tilde{v}$) at $z^*=0.0$ are shown in Figures 32 and 33. The mean velocity results indicate maximum velocities of around $0.034V_B$, while the measured $\tilde{v}$ levels did not exceed $0.039V_B$.

Measurements of the wall static pressure measurements are presented in Figure 34. The distribution of the pressure coefficient is qualitatively similar to that measured in the rectangular duct. The radial pressure gradients in the 45°/45° S-duct are about 0.26 of $\frac{1}{2}\rho V_B^2$, i.e. approximately equal to those in the rectangular S-duct; in the S-diffuser the pressure variation is again equal to that in the rectangular diffuser.

The results are listed in Appendix 1 as Table 2.

4. DISCUSSION

The results allow comparisons to be made with measurements obtained in single S-duct and/or S-diffuser configurations (references 1 and 3, and 4 and 5 respectively) and the determination of the effect of the non-uniform conditions at the inlet of the second S-bend on the flow at the outlet from

10

the ducts. There is considerable asymmetry in the second S-bend in all three configurations, in comparison with the symmetric inlet condition results. The large near-potential flow "core" region present in the flows in the single S-bends is not evident at the exit plane of the ducts in the present configurations. The V velocities at the exit of the rectangular duct have the same predominant direction as those at the exit of the duct of reference 4, but the distribution of the velocities and the size and location of the cross-flow motions is very different. The two cross-flow motions recorded at the exit plane in reference 4 correspond closely to the two vortices located in the corners of the $z^*=1.0$ wall in the present case.

Although no detailed study of flow separation such as that reported in reference 6 was made, no regions of flow detachment were observed throughout the experiments. It is possible that small pockets of incipient separation may exist, but the geometry of all the ducts is such that the high momentum fluid following an approximately straight-line path through the ducts will re-energise the flow and thus will tend to suppress separation near the $z^*=1.0$ wall in the vicinity of the exit of the ducts (i.e. along the inner curved wall in the S-diffuser exit), where separation is more likely to occur (reference 6).

The turbulence levels are in general higher in the present configurations than in the single S-diffusers or S-ducts of the previous investigations. The values of $\tilde{u}$, $\tilde{v}$ and $\tilde{w}$ are higher by around 0.02 V_{B} on average in the present flows. Although the increase in turbulence levels in comparison to single C- or S-shaped bends (e.g. reference 13) is relatively large (0.02 compared with average values of 0.06 V_{B}), the absolute values of the turbulence quantities are still small enough to assume that there are no new qualitative or gross effects of turbulence.

The results are provided in form suitable for the evaluation of numerical calculations of the flows, such as those reported in references 7-10. Laminar flow results can be used to assess the numerical accuracy of the flow calculations, while turbulent flow results can be used to establish the accuracy of the models used for the representation of turbulence. The results show that in the absence of any sizeable recirculation regions, forward marching techniques can be used to calculate the flows, with the associated advantages of computational time and storage economies.

4. CONCLUDING REMARKS

1. Measurements of the velocity characteristics were obtained by laser-Doppler anemometry in laminar and turbulent flow in a out-of-plane double S-bend configuration of rectangular cross-section. Similar measurements were made in the flow in a circular cross-section duct.

2. The results show that the flow patterns at the exit of the ducts are complex, with up to six cross-stream vortical motions in evidence. The flow patterns are strongly asymmetric with large variations and gradients of velocity throughout the duct cross-section. The maximum radial and spanwise cross-stream velocities recorded in turbulent flow in the rectangular duct were 0.11 and 0.05 of the bulk velocity.

3. The results at the exits of the present configurations show that the turbulence levels are higher than at the exits of single S-bends and that there is no near-potential "core" flow region.

4. The laminar and turbulent flow results are suitable for the assessment of numerical methods and turbulence models used for the calculation of these flows and are listed in tabular form for this purpose.

APPENDIX 1

TABULATED DATA

Unless otherwise stated, all quantities listed are normalised with the bulk velocity, V_B, except for the cross-correlations, which are normalised with V_B^2

Table 1.1

Rectangular cross-section duct: Laminar flow data

Re=790

V_B=19.75 mm/s

Centerline variation of U and V

X^*	U	V
0.0	0.949	0.029
0.592	0.960	0.004
0.837	0.970	-0.005
1.452	0.991	-0.027
1.677	0.999	-0.032
1.876	1.001	-0.049
2.057	1.043	-0.060
2.373	1.073	-0.081
2.524	1.142	-0.096
2.662	1.223	-0.109
2.794	1.294	-0.155
2.930	1.339	-0.140
3.073	1.413	-0.121
3.387	1.513	-0.100
3.543	1.505	-0.068
3.755	1.515	-0.035
3.971	1.484	-0.013
4.223	1.427	0.014
4.538	1.406	0.051
4.742	1.382	0.073
5.500	1.408	0.156

U velocities at $X^* = 5.5$

z^*	$r^*=0.1$	0.3	0.5	0.7	0.9
-0.9			0.220	0.379	0.276
-0.8			0.284	0.513	0.469
-0.7		0.130	0.313	0.500	0.619
-0.6	0.136	0.291	0.436	0.444	0.800
-0.5	0.207	0.559	0.569	0.418	0.978
-0.4	0.355	0.760	0.592	0.434	1.093
-0.3	0.448	0.870	0.617	0.604	1.123
-0.2	0.636	0.970	0.799	1.009	1.016
-0.1	0.782	1.071	1.192	1.311	0.772
-0.0	0.843	1.373	1.408	1.253	0.564
0.1	0.926	1.482	1.332	0.960	0.392
0.2	1.001	1.402	1.197	0.817	0.470
0.3	1.090	1.349	1.129	0.959	0.765
0.4	1.174	1.277	1.131	1.107	1.049
0.5	1.284	1.271	1.172	1.239	1.075
0.6	1.187	1.345	1.274	1.327	0.879
0.7	0.777	1.462	1.372	1.131	0.516
0.8	0.301	1.262	1.084	0.640	0.174
0.9		0.596	0.448	0.237	

14

V velocities at X* = 5.5

z*	r*=0.1	0.3	0.5	0.7	0.9
-0.9				0.047	
-0.8			0.006	0.084	0.035
-0.7		0.007	0.012	0.071	0.083
-0.6		0.052	0.035	0.040	0.131
-0.5	-0.012	0.119	0.041	0.012	0.159
-0.4	-0.009	0.150	0.027	0.011	0.160
-0.3	0.008	0.156	0.021	0.023	0.135
-0.2	0.043	0.147	0.044	0.089	0.103
-0.1	0.063	0.155	0.103	0.130	0.036
0.0	0.092	0.176	0.156	0.143	0.007
0.1	0.105	0.187	0.147	0.102	-0.025
0.2	0.119	0.162	0.118	0.090	-0.015
0.3	0.123	0.150	0.100	0.096	0.029
0.4	0.132	0.110	0.073	0.110	0.081
0.5	0.132	0.090	0.075	0.144	0.128
0.6	0.122	0.080	0.107	0.159	0.084
0.7	0.097	0.089	0.122	0.129	0.026
0.8	0.012	0.069	0.077	0.054	-0.013
0.9	-0.007	0.015	0.006	0.009	

	X* = 12.375, r* = 0.5		X* = 16.735, r* = 0.5	
z*	U	V	U	V
-0.9	0.685	0.028	0.673	0.039
-0.8	0.936	0.032	1.091	0.041
-0.7	1.132	0.088	1.189	0.051
-0.6	1.239	0.105	1.201	0.070
-0.5	1.276	0.102	1.178	0.067
-0.4	1.246	0.092	1.146	0.056
-0.3	1.167	0.076	1.123	0.046
-0.2	1.129	0.064	1.073	0.041
-0.1	1.038	0.047	1.062	0.037
0.0	1.011	0.033	1.060	0.033
0.1	0.997	0.033	1.074	0.029
0.2	1.054	0.030	1.111	0.033
0.3	1.111	0.021	1.135	0.033
0.4	1.135	0.024	1.124	0.032
0.5	1.111	0.030	1.074	0.024
0.6	0.984	0.025	0.988	0.021
0.7	0.759	0.022	0.831	0.018
0.8	0.514	0.016	0.583	0.012
0.9	0.237		0.300	

Table 1.2

Rectangular cross-section duct: Turbulent flow data

Re=40,000

$V_\oplus$=1.00 m/s

RECTANGULAR CROSS-SECTION
DOUBLE S-BEND. TURBULENT FLOW:
REYNOLDS NUMBER 40000. WALL PRESSURE MEASUREMENTS

Streamwise Station	Radial Location	Spanwise Location	Pressure Coefficient $C_p = \dfrac{P - P_{ref}}{0.5\rho V_B^2}$
X	r^*	z^*	
-2.0	0.5	-1.0	0.000 (P_{ref})
-1.0	0.0	0.0	-0.071
	1.0	0.0	-0.094
	0.5	1.0	-0.083
+1.1	0.0	0.0	-0.016
	1.0	0.0	-0.271
	0.5	1.0	-0.136
+2.2	0.0	0.0	-0.037
	1.0	0.0	-0.265
	0.5	1.0	-0.154
+3.7	0.0	0.0	-0.318
	1.0	0.0	-0.117
	0.5	1.0	-0.200
+4.4	0.0	0.0	-0.389
	1.0	0.0	-0.134
	0.5	1.0	-0.216
+6.5	0.0	0.0	-0.292
	1.0	0.0	-0.246
	0.5	1.0	-0.244
+6.95	0.5	-1.0	-0.260
	1.0	0.0	-0.265
	0.5	1.0	-0.306
+9.05	0.5	-1.0	-0.287
	1.0	-0.8	-0.295
	1.0	0.0	-0.191
	1.0	0.8	-0.104
	0.5	1.0	-0.067
+10.15	0.5	-1.0	-0.122
	1.0	-0.8	-0.134
	1.0	0.0	-0.104
	1.0	0.8	-0.014
	0.5	1.0	+0.014
+11.25	0.5	-1.0	+0.018
	1.0	-0.8	+0.011
	1.0	0.0	-0.028
	1.0	0.8	-0.067
	0.5	1.0	-0.097
+12.35	0.5	-1.0	+0.078
	1.0	-0.8	+0.073
	1.0	0.0	+0.048
	1.0	0.8	-0.044
	0.5	1.0	-0.090
+14.45	0.5	-1.0	+0.106
	0.5	1.0	+0.094

Centerline variation of $\bar{U}$ and $\bar{V}$

X*	$\bar{U}$	$\bar{V}$
0.0	1.191	0.057
0.592	1.176	0.005
0.837	1.165	-0.014
1.185	1.145	-0.034
1.452	1.131	-0.052
1.677	1.118	-0.064
1.876	1.111	-0.079
2.057	1.100	-0.094
2.378	1.080	-0.121
2.524	1.077	-0.138
2.662	1.065	-0.153
2.794	1.056	-0.160
2.930	1.055	-0.142
3.073	1.049	-0.121
3.225	1.042	-0.109
3.387	1.036	-0.091
3.563	1.026	-0.071
3.755	1.014	-0.058
3.971	0.999	-0.033
4.223	0.993	-0.030
4.538	0.969	-0.001
4.742	0.964	0.010
5.028	0.941	0.052
5.500	0.929	0.055

Centerline variation of $\tilde{u}$, $\tilde{v}$ and $\overline{uv}$

X*	$\tilde{u}$	$\tilde{v}$
0.0	0.015	0.008
0.592	0.018	0.011
0.837	0.019	0.012
1.185	0.019	0.017
1.452	0.020	0.013
1.677	0.021	0.017
1.876	0.023	0.017
2.057	0.025	0.017
2.378	0.026	0.020
2.524	0.030	0.023
2.662	0.032	0.024
2.794	0.038	0.023
2.930	0.039	0.024
3.073	0.041	0.025
3.225	0.046	0.031
3.387	0.047	0.032
3.563	0.052	0.033
3.755	0.055	0.032
4.223	0.056	0.033
4.742	0.060	0.041
5.500	0.065	0.042

X*	$\overline{uv}$
0.0	0.00001
0.592	-0.00003
0.837	-0.00005
1.185	-0.00002
1.677	-0.00002
2.057	-0.00002
2.378	-0.00008
2.524	-0.00014
2.662	-0.00019
2.794	-0.00012
2.930	-0.00024
3.073	-0.00015
3.225	-0.00001
3.387	-0.00009
3.563	-0.00005
3.755	-0.00000
4.223	0.00017
4.742	0.00041
5.500	0.00077

$\overline{U}$ velocities at X = 0.0 (station 1)

z*	r=0.1	0.3	0.5	0.7	0.9
0.0	0.975	1.112	1.118	1.133	1.008
0.1	0.950	1.108	1.116	1.136	0.991
0.2	0.942	1.112	1.117	1.135	0.995
0.3	0.956	1.111	1.115	1.136	1.003
0.4	0.978	1.101	1.117	1.140	1.015
0.5	0.973	1.107	1.114	1.135	1.015
0.6	0.961	1.096	1.103	1.125	1.023
0.65	0.953	1.072	1.062	1.105	1.012
0.7	0.953	1.043	1.033	1.092	1.005
0.75	0.941	0.999	1.025	1.054	0.998
0.8	0.939	0.955	0.982	1.015	0.974
0.85	0.915	0.895	0.902	0.960	0.922
0.9	0.864	0.826	0.803	0.905	0.756
0.925	0.831	0.736	0.689	0.856	0.689
0.95	0.720	0.596	0.602	0.786	0.456

$\tilde{u}$ velocities at X = 0.0 (station 1)

z*	r*=0.1	0.3	0.5	0.7	0.9
0.0	0.050	0.007	0.006	0.007	0.045
0.1	0.050	0.007	0.007	0.007	0.049
0.2	0.050	0.007	0.006	0.007	0.048
0.3	0.053	0.007	0.007	0.007	0.049
0.4	0.052	0.008	0.007	0.008	0.046
0.5	0.055	0.009	0.010	0.011	0.046
0.6	0.053	0.020	0.019	0.015	0.047
0.65	0.055	0.034	0.036	0.027	0.044
0.7	0.056	0.041	0.041	0.032	0.047
0.75	0.054	0.051	0.043	0.042	0.045
0.8	0.049	0.055	0.051	0.047	0.042
0.85	0.050	0.060	0.057	0.056	0.043
0.9	0.053	0.064	0.067	0.058	0.058
0.925	0.057	0.072	0.075	0.061	0.086
0.95	0.078	0.093	0.111	0.066	0.118

$\overline{U}$ and $\tilde{u}$ velocities at X = 5.5 (station 2)

z*	$\overline{U}$					$\tilde{u}$				
	r*=0.1	0.3	0.5	0.7	0.9	0.1	0.3	0.5	0.7	0.9
-.95	0.828	0.895	0.855	0.813	0.738	0.084	0.082	0.082	0.077	0.057
-.925	0.919	0.944	0.915	0.862	0.766	0.071	0.078	0.075	0.072	0.056
-.9	0.967	1.030	0.957	0.906	0.800	0.062	0.067	0.070	0.069	0.060
-.85	1.004	1.088	1.023	0.964	0.845	0.058	0.054	0.060	0.056	0.058
-.8	1.040	1.129	1.066	1.005	0.885	0.053	0.041	0.048	0.047	0.050
-.75	1.039	1.154	1.089	1.024	0.914	0.054	0.035	0.042	0.046	0.046
-.7	1.037	1.171	1.115	1.047	0.917	0.054	0.028	0.039	0.040	0.042
-.65	1.039	1.184	1.131	1.059	0.911	0.054	0.024	0.035	0.039	0.046
-.6	1.040	1.193	1.153	1.071	0.898	0.054	0.018	0.028	0.039	0.050
-.5	1.048	1.197	1.175	1.076	0.841	0.055	0.013	0.018	0.045	0.054
-.4	1.068	1.201	1.177	1.061	0.772	0.052	0.012	0.011	0.053	0.055
-.3	1.095	1.200	1.182	1.053	0.714	0.050	0.010	0.008	0.053	0.055
-.2	1.104	1.202	1.182	1.061	0.716	0.046	0.009	0.008	0.050	0.061
-.1	1.107	1.201	1.181	1.068	0.758	0.047	0.010	0.008	0.046	0.062
0.0	1.091	1.199	1.184	1.077	0.758	0.048	0.011	0.008	0.043	0.063
0.1	1.070	1.198	1.185	1.070	0.727	0.051	0.012	0.009	0.045	0.064
0.2	1.055	1.197	1.186	1.062	0.717	0.049	0.013	0.009	0.047	0.057
0.3	1.041	1.197	1.185	1.065	0.754	0.053	0.013	0.010	0.050	0.056
0.4	1.050	1.197	1.183	1.070	0.815	0.052	0.013	0.013	0.047	0.055
0.5	1.052	1.195	1.165	1.077	0.871	0.055	0.016	0.024	0.042	0.053
0.6	1.041	1.191	1.127	1.058	0.910	0.055	0.017	0.036	0.041	0.046
0.65	1.034	1.184	1.106	1.040	0.913	0.057	0.021	0.038	0.041	0.044
0.7	1.026	1.177	1.088	1.020	0.904	0.059	0.024	0.040	0.045	0.045
0.75	1.017	1.160	1.071	0.994	0.876	0.057	0.030	0.040	0.046	0.050
0.8	1.008	1.142	1.050	0.961	0.848	0.055	0.036	0.045	0.054	0.056
0.85	0.980	1.080	1.007	0.897	0.799	0.059	0.051	0.057	0.056	0.059
0.9	0.951	1.018	0.890	0.827	0.693	0.062	0.066	0.072	0.067	0.044
0.925	0.901		0.591	0.771		0.069		0.113	0.066	
0.95	0.787		0.390			0.074				

$\overline{U}$ and $\tilde{u}$ velocities at $X^* = 0.0$ (station 3)

z*	$\overline{U}$ r*=0.3	0.7	$\tilde{u}$ 0.3	0.7
-.95	0.942	0.897	0.074	0.074
-.925	0.986	0.942	0.072	0.072
-.9	1.024	0.969	0.069	0.071
-.85	1.091	1.022	0.061	0.063
-.8	1.135	1.064	0.052	0.057
-.75	1.170	1.094	0.042	0.047
-.7	1.190	1.101	0.032	0.044
-.65	1.195	1.111	0.026	0.046
-.6	1.198	1.108	0.023	0.052
-.5	1.200	1.083	0.021	0.060
-.4	1.199	1.062	0.022	0.066
-.3	1.197	1.040	0.020	0.067
-.2	1.192	1.037	0.018	0.068
-.1	1.191	1.048	0.019	0.070
0.0	1.184	1.050	0.020	0.064
0.1	1.177	1.053	0.023	0.065
0.2	1.177	1.052	0.021	0.065
0.3	1.176	1.052	0.021	0.065
0.4	1.173	1.064	0.020	0.062
0.5	1.173	1.075	0.018	0.053
0.6	1.166	1.070	0.023	0.044
0.65	1.158	1.058	0.025	0.045
0.7	1.146	1.037	0.031	0.051
0.75	1.122	0.999	0.043	0.057
0.8	1.081	0.957	0.058	0.066
0.85	1.020	0.902	0.074	0.073
0.9	0.936	0.833	0.078	0.075
0.925	0.888	0.797	0.079	0.080
0.95	0.843	0.750	0.080	0.084

21

$\overline{U}$ velocities at X* = 5.5 (station 4)

z*	r*=0.1	0.3	0.5	0.7	0.9
-0.9	0.315	0.338	0.362	0.508	0.490
-0.8	0.348	0.353	0.373	0.540	0.513
-0.7	0.395	0.367	0.425	0.608	0.526
-0.6	0.453	0.411	0.500	0.674	0.511
-0.5	0.499	0.489	0.594	0.705	0.480
-0.4	0.534	0.592	0.706	0.696	0.457
-0.3	0.563	0.698	0.814	0.687	0.478
-0.2	0.587	0.778	0.882	0.672	0.534
-0.1	0.611	0.830	0.915	0.685	0.600
0.0	0.632	0.860	0.929	0.703	0.662
0.1	0.668	0.894	0.937	0.751	0.711
0.2	0.708	0.920	0.955	0.799	0.753
0.3	0.754	0.946	0.977	0.840	0.786
0.4	0.801	0.965	0.994	0.895	0.807
0.5	0.840	0.990	1.010	0.938	0.810
0.6	0.864	1.005	1.008	0.941	0.786
0.7	0.865	0.995	0.962	0.903	0.747
0.8	0.823	0.936	0.882	0.821	0.685
0.9	0.698	0.780	0.734	0.678	0.596

$\tilde{u}$ velocities at X* = 5.5 (station 4)

z*	r*=0.1	0.3	0.5	0.7	0.9
-0.9	0.052	0.054	0.068	0.061	0.043
-0.8	0.060	0.064	0.082	0.083	0.064
-0.7	0.067	0.072	0.099	0.085	0.071
-0.6	0.070	0.082	0.107	0.076	0.074
-0.5	0.071	0.092	0.112	0.073	0.074
-0.4	0.069	0.093	0.104	0.077	0.065
-0.3	0.070	0.083	0.084	0.079	0.068
-0.2	0.069	0.067	0.064	0.077	0.070
-0.1	0.068	0.061	0.062	0.072	0.069
0.0	0.068	0.059	0.065	0.071	0.066
0.1	0.067	0.057	0.066	0.070	0.065
0.2	0.066	0.054	0.061	0.070	0.065
0.3	0.065	0.049	0.052	0.066	0.066
0.4	0.064	0.044	0.041	0.060	0.066
0.5	0.062	0.036	0.032	0.051	0.070
0.6	0.064	0.030	0.035	0.054	0.071
0.7	0.066	0.039	0.054	0.066	0.073
0.8	0.067	0.059	0.069	0.074	0.069
0.9	0.070	0.075	0.078	0.079	0.059

∇ velocities at X* = 5.5 (station 4)

z*	r*=0.1	0.3	0.5	0.7	0.9
-0.9	0.032	0.009	-0.001	0.034	
-0.8	0.051	0.010	0.001	0.082	0.034
-0.7	0.054	0.003	0.015	0.095	0.024
-0.6	0.058	0.004	0.039	0.106	0.016
-0.5	0.054	0.015	0.059	0.098	0.008
-0.4	0.043	0.036	0.068	0.071	0.013
-0.3	0.038	0.045	0.080	0.053	0.025
-0.2	0.033	0.050	0.076	0.031	0.040
-0.1	0.035	0.058	0.070	0.025	0.058
0.0	0.033	0.051	0.059	0.020	0.069
0.1	0.041	0.052	0.043	0.023	0.074
0.2	0.042	0.045	0.043	0.026	0.076
0.3	0.050	0.041	0.035	0.028	0.066
0.4	0.047	0.037	0.037	0.034	0.048
0.5	0.042	0.035	0.039	0.034	0.036
0.6	0.035	0.037	0.041	0.033	0.016
0.7	0.020	0.035	0.034	0.034	0.006
0.8	0.004	0.029	0.027	0.023	-0.007
0.9	-0.019	0.014	0.010	0.014	-0.029

$\tilde{v}$ velocities at X* = 5.5 (station 4)

z*	r*=0.1	0.3	0.5	0.7	0.9
-0.9	0.045	0.037	0.053	0.057	
-0.8	0.050	0.048	0.051	0.055	0.052
-0.7	0.050	0.045	0.052	0.058	0.055
-0.6	0.049	0.054	0.064	0.050	0.055
-0.5	0.047	0.056	0.056	0.053	0.053
-0.4	0.050	0.059	0.061	0.052	0.054
-0.3	0.043	0.054	0.058	0.055	0.053
-0.2	0.049	0.047	0.044	0.058	0.052
-0.1	0.051	0.056	0.039	0.060	0.053
0.0	0.049	0.043	0.042	0.059	0.050
0.1	0.049	0.040	0.040	0.058	0.052
0.2	0.047	0.039	0.032	0.055	0.049
0.3	0.045	0.032	0.034	0.054	0.045
0.4	0.045	0.034	0.027	0.049	0.044
0.5	0.043	0.026	0.024	0.046	0.035
0.6	0.041	0.022	0.024	0.038	0.034
0.7	0.038	0.028	0.029	0.035	0.032
0.8	0.038	0.029	0.030	0.035	0.017
0.9	0.033	0.037	0.039	0.057	

uv cross-correlations at X* = 5.5

z*	r*=0.1	0.3	0.5	0.7	0.9
-0.9	0.00071	0.00055	0.00020	0.00139	
-0.8	0.00117	0.00065	0.00148	0.00174	0.00098
-0.7	0.00134	0.00084	0.00248	0.00201	0.00074
-0.6	0.00126	0.00159	0.00294	0.00119	0.00039
-0.5	0.00105	0.00247	0.00319	0.00098	-0.00022
-0.4	0.00099	0.00293	0.00308	0.00082	0.00012
-0.3	0.00046	0.00231	0.00204	0.00070	0.00108
-0.2	0.00059	0.00156	0.00102	0.00092	0.00155
-0.1	0.00062	0.00081	0.00072	0.00131	0.00178
0.0	0.00054	0.00068	0.00077	0.00150	0.00145
0.1	0.00063	0.00046	0.00096	0.00169	0.00146
0.2	0.00057	0.00046	0.00063	0.00181	0.00154
0.3	0.00076	0.00032	0.00068	0.00165	0.00141
0.4	0.00086	0.00032	0.00037	0.00128	0.00133
0.5	0.00058	0.00016	0.00020	0.00090	0.00096
0.6	0.00051	0.00007	-0.00002	0.00025	0.00058
0.7	0.00021	-0.00010	-0.00018	-0.00006	0.00032
0.8	-0.00005	-0.00022	-0.00026	-0.00028	0.00010
0.9	-0.00065	-0.00065	-0.00075	-0.00014	-0.00018

Ū, V̄, ũ, ṽ and $\overline{uv}$ in the downstream tangent

z*	X* = 12.375, r* = 0.5					X* = 16.735, r* = 0.5				
	Ū	V̄	ũ	ṽ	$\overline{uv}$	Ū	V̄	ũ	ṽ	$\overline{uv}$
-0.9	0.605	0.017	0.063	0.038	0.00024	0.586	0.023	0.024	0.039	-0.00010
-0.8	0.629	0.024	0.059	0.043	0.00069	0.647	0.035	0.053	0.031	0.00032
-0.7	0.645	0.031	0.057	0.049	0.00091	0.676	0.032	0.049	0.039	0.00043
-0.6	0.661	0.029	0.063	0.043	0.00114	0.700	0.032	0.051	0.041	0.00071
-0.5	0.694	0.035	0.067	0.044	0.00122	0.721	0.037	0.053	0.039	0.00073
-0.4	0.730	0.043	0.068	0.045	0.00128	0.746	0.039	0.052	0.043	0.00084
-0.3	0.764	0.042	0.064	0.047	0.00112	0.767	0.040	0.054	0.043	0.00079
-0.2	0.799	0.047	0.062	0.043	0.00110	0.789	0.042	0.053	0.039	0.00073
-0.1	0.828	0.043	0.061	0.046	0.00099	0.809	0.040	0.055	0.041	0.00065
0.0	0.854	0.041	0.058	0.044	0.00088	0.828	0.040	0.054	0.041	0.00065
0.1	0.879	0.038	0.058	0.042	0.00084	0.847	0.038	0.052	0.040	0.00035
0.2	0.902	0.040	0.054	0.039	0.00060	0.854	0.036	0.052	0.038	0.00014
0.3	0.918	0.035	0.051	0.038	0.00027	0.846	0.030	0.053	0.036	-0.00007
0.4	0.908	0.034	0.057	0.039	-0.00045	0.823	0.031	0.056	0.038	-0.00059
0.5	0.860	0.036	0.070	0.040	-0.00118	0.790	0.032	0.059	0.042	-0.00082
0.6	0.789	0.032	0.077	0.041	-0.00138	0.756	0.037	0.058	0.048	-0.00086
0.7	0.711	0.033	0.076	0.040	-0.00134	0.697		0.053		
0.8	0.642	0.029	0.073	0.034	-0.00108	0.634		0.048		
0.9	0.576	0.018	0.065	0.028	-0.00065	0.556		0.040		

Table 2

Circular cross-section duct data

Re=48,000

V_B=1.00 m/s

CIRCULAR CROSS-SECTION
DOUBLE S-BEND.   TURBULENT FLOW:
REYNOLDS NUMBER 48000.   WALL PRESSURE MEASUREMENTS

Streamwise Station	Radial Location	Spanwise Location	Pressure Coefficient $C_p = \dfrac{P-P_{ref}}{0.5\rho V_B^2}$
X	r*	z*	
-1.0	0.5	-1.0	0.000 (Pref)
	0.0	0.0	+0.004
	1.0	0.0	-0.012
+0.55	0.5	-1.0	-0.027
	0.0	0.0	+0.088
	1.0	0.0	-0.166
+1.65	0.5	-1.0	+0.055
	0.0	0.0	+0.083
	1.0	0.0	-0.191
+3.85	0.5	1.0	-0.111
	0.0	0.0	+0.035
	1.0	0.0	-0.221
+4.95	0.5	1.0	-0.143
	0.0	0.0	-0.012
+5.13	1.0	0.0	-0.202
+6.05	0.5	1.0	-0.168
	0.0	0.0	-0.309
	1.0	0.0	-0.092
+7.15	0.5	1.0	-0.191
	0.0	0.0	-0.341
	1.0	0.0	-0.074
+9.35	0.5	-1.0	-0.233
	0.0	0.0	-0.386
	1.0	0.0	-0.110
+10.45	0.5	-1.0	-0.274
	1.0	0.0	-0.136
+10.63	0.0	0.0	-0.364
+12.10	0.5	-1.0	-0.244
	1.0	0.0	-0.129
	0.5	1.0	-0.025
+13.20	0.5	-1.0	-0.127
	1.0	0.0	-0.042
	0.5	1.0	+0.055
+14.3	0.5	-1.0	+0.064
	1.0	0.0	+0.034
	0.5	1.0	-0.083
+15.4	0.5	-1.0	+0.138
	1.0	0.0	+0.097
	0.5	1.0	-0.021
+17.5	0.5	-1.0	+0.130
	1.0	0.0	+0.131
	0.0	1.0	+0.138

Centerline variation of $\overline{U}$ and $\tilde{u}$

X*	$\overline{U}$	$\tilde{u}$
0.150	0.956	0.047
0.540	0.955	0.053
0.764	0.943	0.052
1.325	0.933	0.051
1.531	0.923	0.047
1.712	0.920	0.049
1.877	0.916	0.049
2.029	0.905	0.043
2.303	0.909	0.049
2.429	0.906	0.047
2.548	0.902	0.045
2.886	0.888	0.047
3.002	0.895	0.049
3.124	0.889	0.046
3.252	0.894	0.048
3.471	0.879	0.046
3.535	0.887	0.046
3.623	0.873	0.046
3.691	0.881	0.046
3.788	0.855	0.040
3.862	0.874	0.044
3.969	0.848	0.041
4.175	0.841	0.043
4.736	0.838	0.042
4.960	0.831	0.042
5.270	0.818	0.040
5.350	0.816	0.041

Centerline variation of $\overline{V}$ and $\tilde{v}$

X*	$\overline{V}$	$\tilde{v}$
0.150	0.002	0.043
0.540	−0.015	0.040
0.764	−0.017	0.041
1.325	−0.019	0.041
1.531	−0.021	0.042
1.712	−0.026	0.043
1.877	−0.029	0.042
2.029	−0.033	0.041
2.303	−0.034	0.038
2.429	−0.036	0.038
2.548	−0.040	0.039
2.886	−0.050	0.041
3.002	−0.043	0.041
3.124	−0.039	0.041
3.252	−0.035	0.040
3.471	−0.020	0.039
3.535	−0.017	0.040
3.623	−0.016	0.044
3.691	−0.014	0.039
3.788	−0.013	0.042
3.862	−0.011	0.041
3.969	−0.009	0.042
4.175	−0.005	0.042
4.736	0.001	0.042
4.960	0.010	0.041
5.270	0.012	0.040
5.350	0.014	0.041

U̅ and ũ velocities at X* = 5.5

U denotes U̅ in m/s
UD denotes ũ in m/s

R(MM)	10.52	13.18	15.84	18.49	21.15	23.80	26.46	29.11	31.77
Z(MM)	20.32	20.64	20.97	21.30	21.62	21.95	22.28	22.60	22.93
U(M/S)	.745	.793	.811	.825	.848	.846	.844	.849	.822
UD(M/S)	.036	.035	.027	.025	.026	.025	.025	.024	.025

R(MM)	4.35	7.02	9.69	12.36	15.04	17.71	20.38	23.06	25.73	28.40	31.07
Z(MM)	10.12	10.24	10.36	10.48	10.60	10.72	10.84	10.96	11.08	11.20	11.32
U(M/S)	.648	.750	.791	.808	.816	.822	.823	.826	.829	.838	.848
UD(M/S)	.056	.048	.039	.037	.035	.034	.038	.037	.038	.039	.039

R(MM)	33.75	36.42	39.09	41.77	44.44	47.11	49.79	52.46
Z(MM)	11.44	11.56	11.68	11.80	11.92	12.04	12.16	12.28
U(M/S)	.852	.857	.857	.852	.841	.823	.783	.698
UD(M/S)	.041	.040	.040	.043	.046	.045	.056	.066

R(MM)	2.44	5.12	7.79	10.47	13.15	15.82	18.50	21.17	23.85	26.52	29.20
Z(MM)	.00	.00	.00	.00	.00	.00	.00	.00	.00	.00	.00
U(M/S)	.631	.701	.741	.763	.781	.795	.799	.802	.813	.813	.817
UD(M/S)	.052	.046	.044	.044	.041	.036	.035	.033	.040	.041	.040

R(MM)	31.88	34.55	37.23	39.90	42.58	45.25	47.93	50.60	53.28	55.96
Z(MM)	.00	.00	.00	.00	.00	.00	.00	.00	.00	.00
U(M/S)	.814	.813	.814	.819	.808	.797	.767	.731	.680	.625
UD(M/S)	.042	.042	.042	.045	.045	.052	.057	.059	.061	.069

R(MM)	4.35	7.02	9.69	12.36	15.04	17.71	20.38	23.06	25.73	28.40	31.07
Z(MM)	-10.12	-10.24	-10.36	-10.48	-10.60	-10.72	-10.84	-10.96	-11.08	-11.20	-11.32
U(M/S)	.590	.638	.655	.669	.672	.678	.681	.687	.687	.689	.694
UD(M/S)	.058	.055	.052	.057	.074	.074	.084	.086	.089	.089	.088

R(MM)	33.75	36.42	39.09	41.77	44.44	47.11	49.79	52.46
Z(MM)	-11.44	-11.56	-11.68	-11.80	-11.92	-12.04	-12.16	-12.28
U(M/S)	.685	.688	.692	.680	.663	.622	.570	.487
UD(M/S)	.097	.097	.093	.088	.079	.087	.078	.076

R(MM)	10.52	13.18	15.84	18.49	21.15	23.80
Z(MM)	-20.32	-20.64	-20.97	-21.30	-21.62	-21.95
U(M/S)	.485	.500	.497	.466	.455	.420
UD(M/S)	.043	.041	.046	.044	.047	.040

$\overline{V}$ and $\tilde{v}$ at $z^* = 0$, $X^* = 5.5$

V denotes $\overline{V}$ in m/s; VD denotes $\tilde{v}$ in m/s

R(MM) %	5.24	7.39	9.59	11.85	14.15	16.51	18.92	21.39	23.92
V(M/S) %	-.005	.016	.021	.019	.022	.025	.033	.034	.034
VD(M/S)%	.036	.034	.033	.033	.032	.035	.033	.032	.034

R(MM) %	26.51	29.15	31.86	34.63	37.46	40.36	43.33	46.36
V(M/S) %	.029	.012	.004	-.005	-.009	-.011	-.015	-.027
VD(M/S)%	.038	.040	.039	.036	.034	.037	.039	.039

APPENDIX 2

Definition of symbols

C_p	Pressure coefficient
D	Hydraulic diameter at the duct inlet
P	Pressure at the wall
P_{ref}	Reference value of P
r	Coordinate direction perpendicular to the duct centerline in the horizontal plane
r_i	Radius of curvature of wall nearest to the center of curvature
r_o	Radius of curvature of wall furthest from the center of curvature
r^*	Normalised radial coordinate, $r^* \equiv (r - r_o)/(r_i - r_o)$, in the direction defined in Figures 1 and 2
R_c	Mean radius of curvature : $R_c \equiv \frac{1}{2}(r_i + r_o)$
Re	Reynolds number based on V_B and D
U, u	Streamwise mean and r.m.s. velocity components
uv, uw	Cross-correlations between u and v, and u and w respectively
V, v	Mean and r.m.s. velocity in the local radial direction (r^* in the first S-bend and z^* in the second S-bend)
V_B	Bulk mean velocity (mass flow rate/inlet cross-sectional area)
W, w	Mean and r.m.s. velocity in the local spanwise direction (z^* in the first S-bend and r^* in the second S-bend)
X	Streamwise coordinate, measured in hydraulic diameters along the duct centerline from the inlet of the first S-bend
X^*	Streamwise coordinate, measured in hydraulic diameters along the duct centerline from the inlet of the second S-bend
z	Coordinate direction perpendicular to the duct centerline in vertical plane
z_h	Duct half-width
z^*	Normalised coordinate: $z^* \equiv z/z_h$

32

REFERENCES

1. Taylor, A.M.K.P., Whitelaw, J.H. and Yianneskis, M. (1982a). Developing flow in S-shaped ducts. Part I - Square cross-section duct. NASA Contractor Report 3550.

2. Bansod, P. and Bradshaw, P. (1972). The flow in S-shaped ducts. Aero. Quarterly, **23**, 131.

3. Taylor, A.M.K.P., Whitelaw, J.H. and Yianneskis, M. (1984). Developing flow in S-shaped ducts. Part II - Circular cross-section duct. NASA Contractor Report 3759.

4. Rojas, J., Whitelaw, J.H. and Yianneskis, M. (1983a). Developing flow in S-shaped diffusers. Part I - Rectangular cross-section diffuser. NASA Contractor Report.

5. Rojas, J., Whitelaw, J.H. and Yianneskis, M. (1983b). Developing flow in S-shaped diffusers. Part II - Circular cross-section diffuser. NASA Contractor Report.

6. Rojas, J., Whitelaw, J.H. and Yianneskis, M. (1984). Inlet condition effects on incipient separation in curved diffusers. NASA Contractor Report.

7. Levy, R., McDonald, H., Briley, W.R. and Kreskovsky, J.P. (1980). A three-dimensional turbulent compressible subsonic duct flow analysis for use with constructed coordinate systems. AIAA Paper 80-1398.

8. Towne, C. and Anderson, B.H. (1981). Numerical simulation of flows in curved diffusers with cross-sectional transitioning using a three-dimensional viscous analysis. AIAA Paper 81-0003.

9. Levy, R., Briley, W.R. and McDonald, H. (1983). Viscous primary/secondary flow analysis for use with nonorthogonal coordinate systems. AIAA Paper 83-0556.

10. Towne, C. (1984). Computation of viscous flow in curved ducts and comparison with experimental data. AIAA Paper 84-0531.

11. Taylor, A.M.K.P., Whitelaw, J.H. and Yianneskis, M. (1981). Measurements of laminar and turbulent flow in a curved duct with thin inlet boundary layers. NASA Contractor Report 3367.

12. Taylor, A.M.K.P., Whitelaw, J.H. and Yianneskis, M. (1982b). Curved ducts with strong secondary motion: Velocity measurements of developing laminar and turbulent flow. J. Fluids Engng., **104**, 350.

13. Rojas, J., Whitelaw, J.H., and Yianneskis, M. (1983c). Flow in sigmoid diffusers of moderate curvature. Proc. Fourth Symp. on Turbulent Shear Flows, Karlsruhe, Germany, September 1983.

Figures

In the computer-generated plots following:

$$VB \text{ refers to } V_B$$
$$X* \text{ refers to } X^*$$
$$Z* \text{ refers to } z^*$$
$$\text{RMS-U refers to } \tilde{u}/V_B$$
$$\text{RMS-V refers to } \tilde{v}/V_B$$
$$\text{RMS-W refers to } \tilde{w}/V_B$$
$$UV \text{ refers to } \overline{uv}$$
$$UW \text{ refers to } \overline{uw}$$

SIDE VIEW

300

Flow

S — duct

Spacer

S — diffuser

X

z* X*

z*

98

215

2000

40

60

32

TOP VIEW

□ 40

Station ①

$r_i = 260$

$r_o = 300$

②

③

④

r*

r* X*

X*

42

□ 40

Flow

r*

X

215
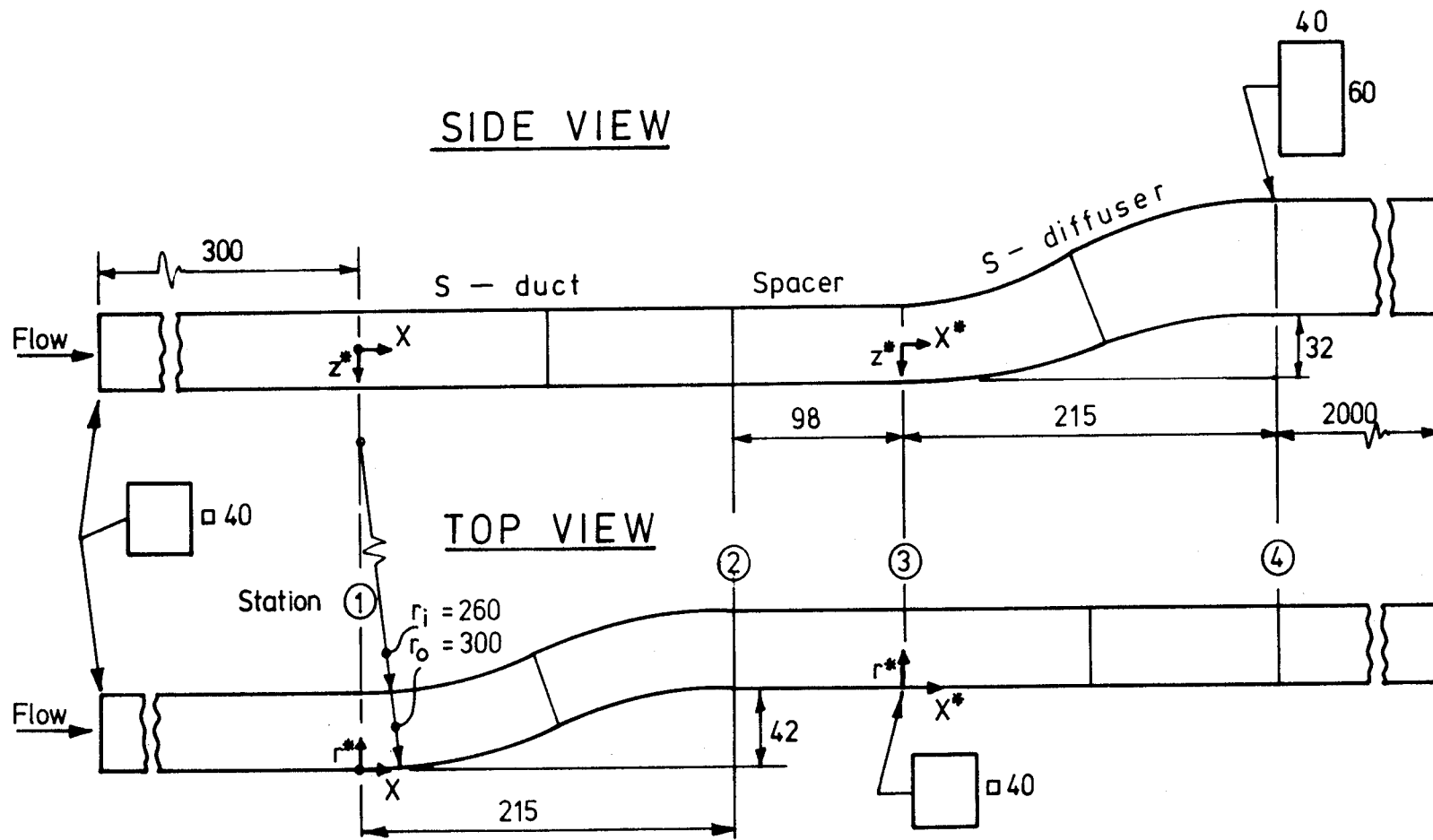
Dimensions in mm — not to scale

Figure 1 (a).   Rectangular duct: Flow configuration and coordinate system

Diffuser exit notation

Flow is emerging from page
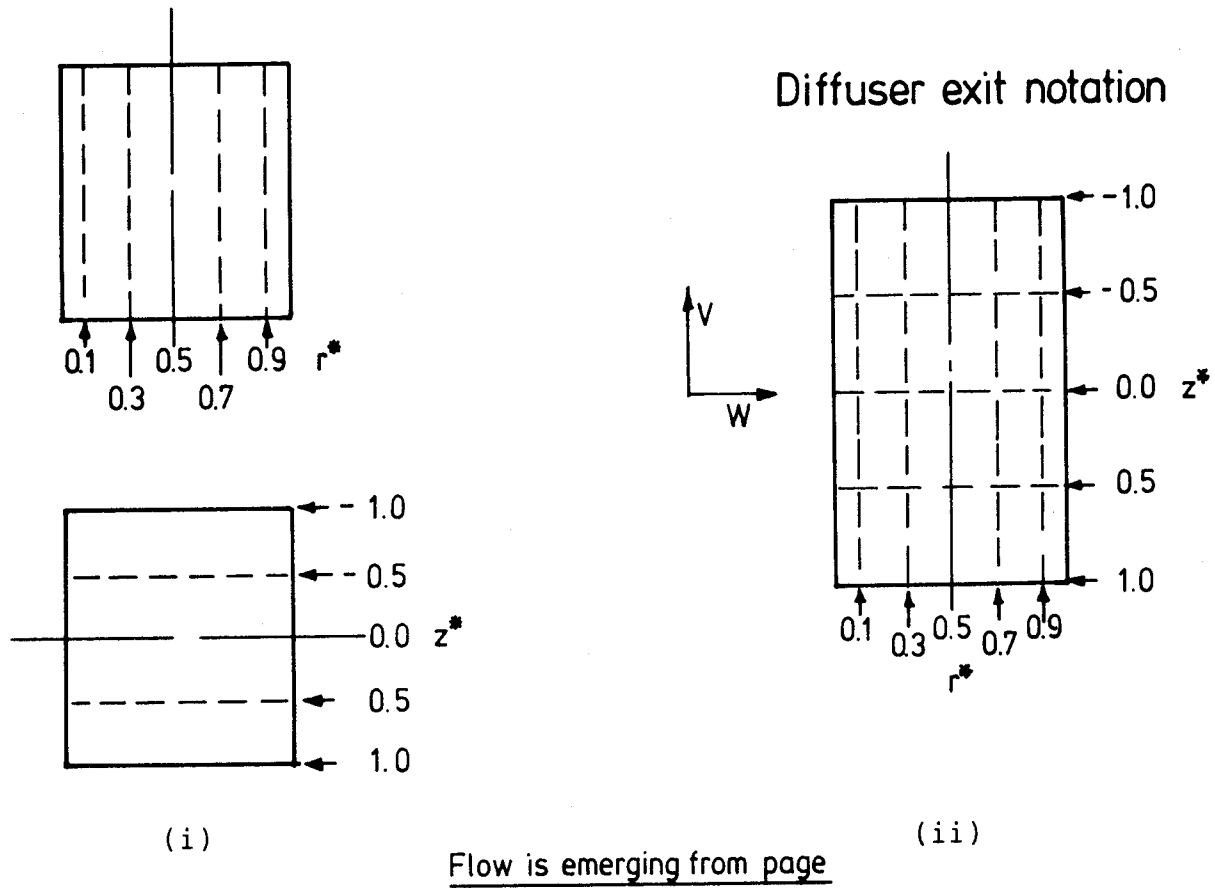
Figure 1 (b).   Rectangular duct: Cross-stream coordinate notation.

(i)   S-duct and spacer
(ii)   S-diffuser exit

SIDE VIEW

210

Flow

S - duct

S-diffuser

58.8

z* X

z* X*

20.2

257.2

18,20

TOP VIEW

r*

X*

48

48

$r_i = 312$

$r_o = 360$

196.8

r*

Flow

X

475.2
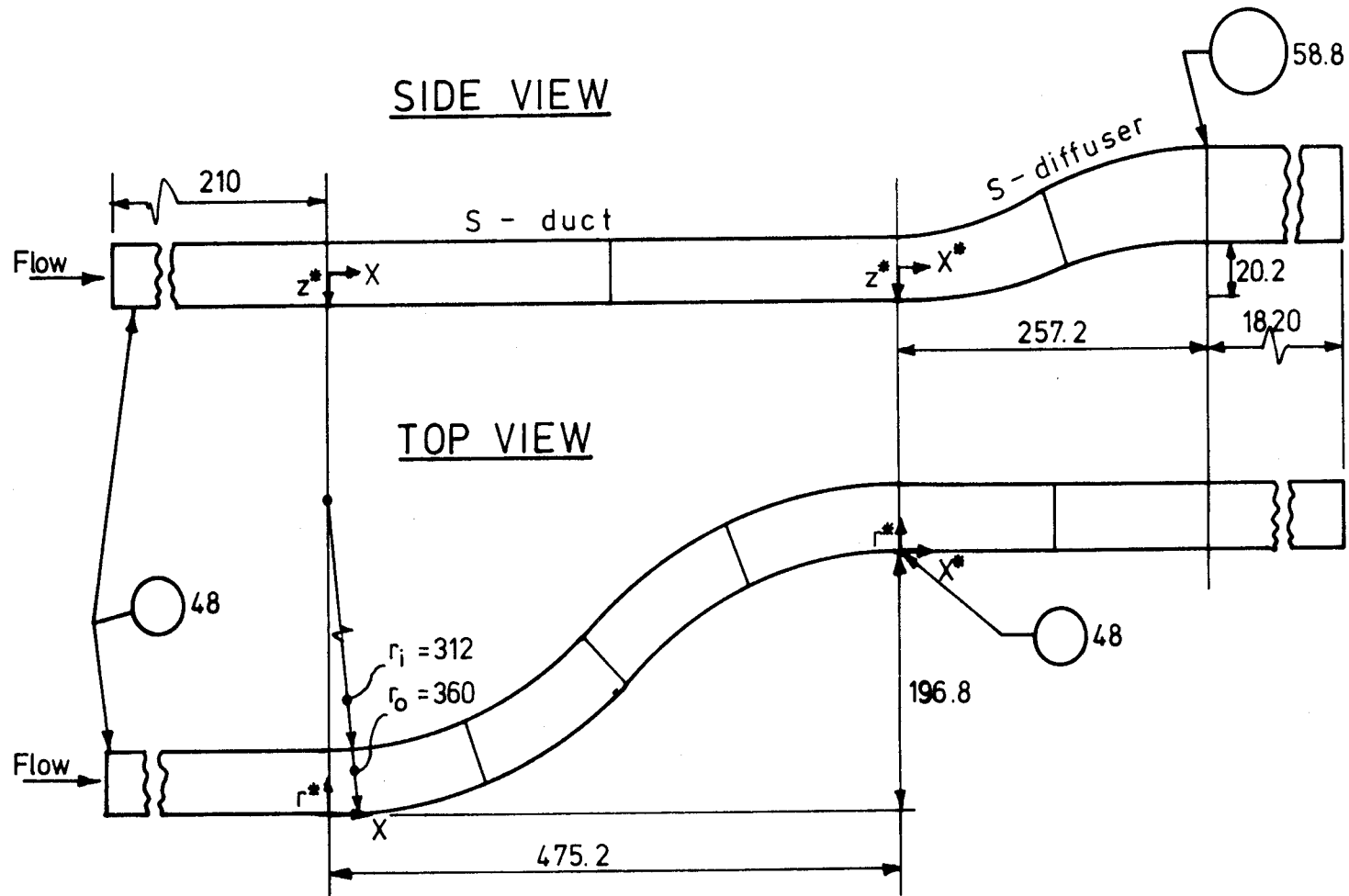
Dimensions in mm – not to scale

Figure 2. Circular duct: Flow configuration and coordinate system
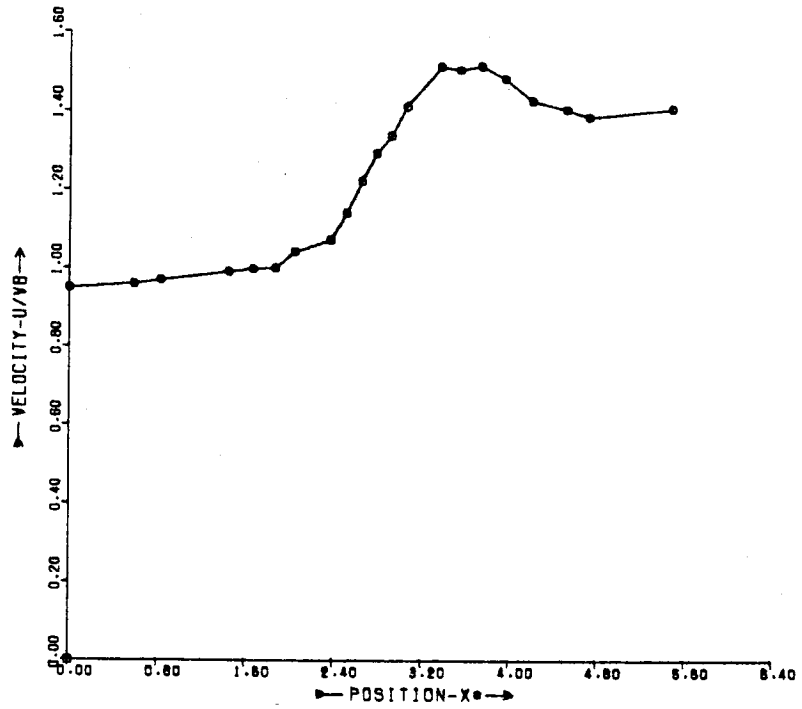
Figure 3.   Rectangular diffuser, laminar flow:
            Centerline variation of U velocity.
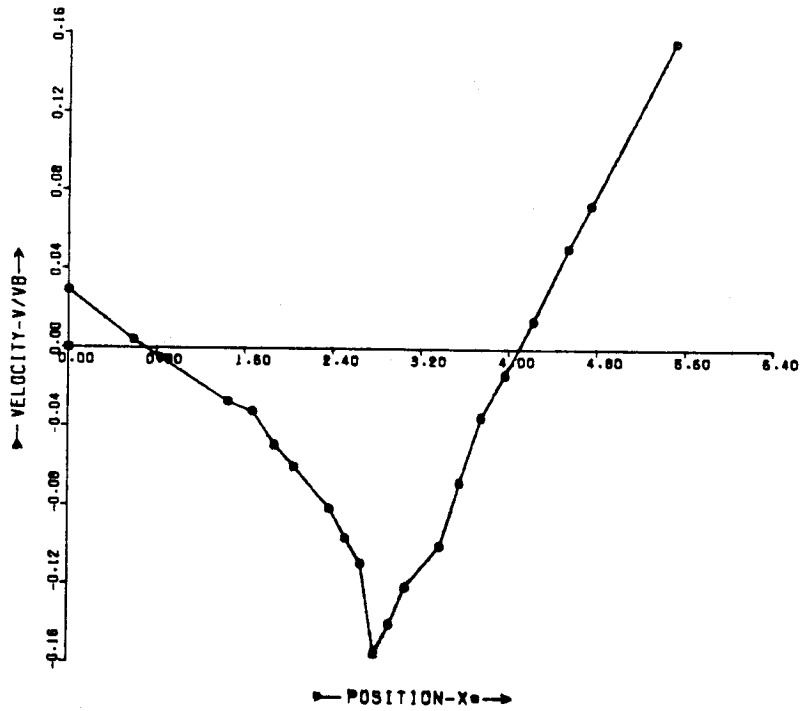
Figure 4.   Rectangular diffuser, laminar flow:
            Centerline variation of V velocity

38
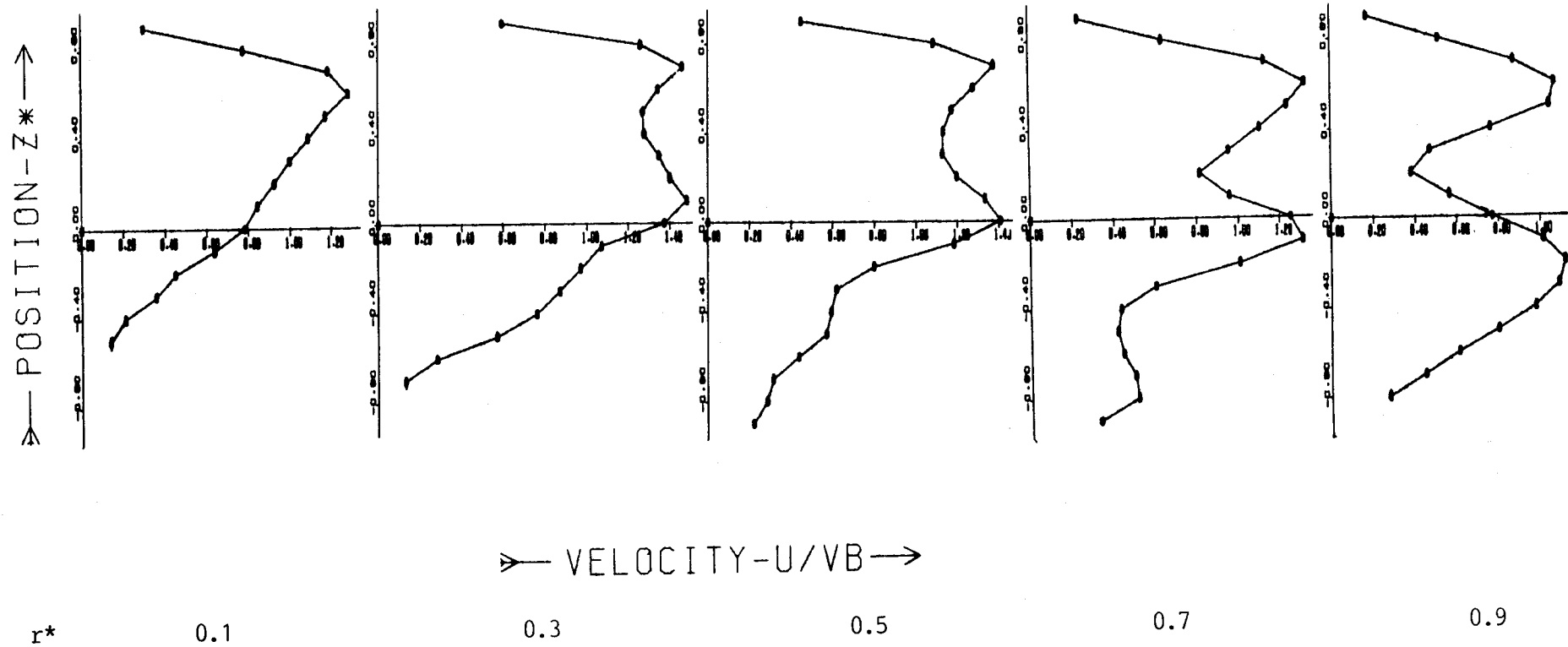
Figure 5. Rectangular diffuser, laminar flow: Profiles of U at the exit plane
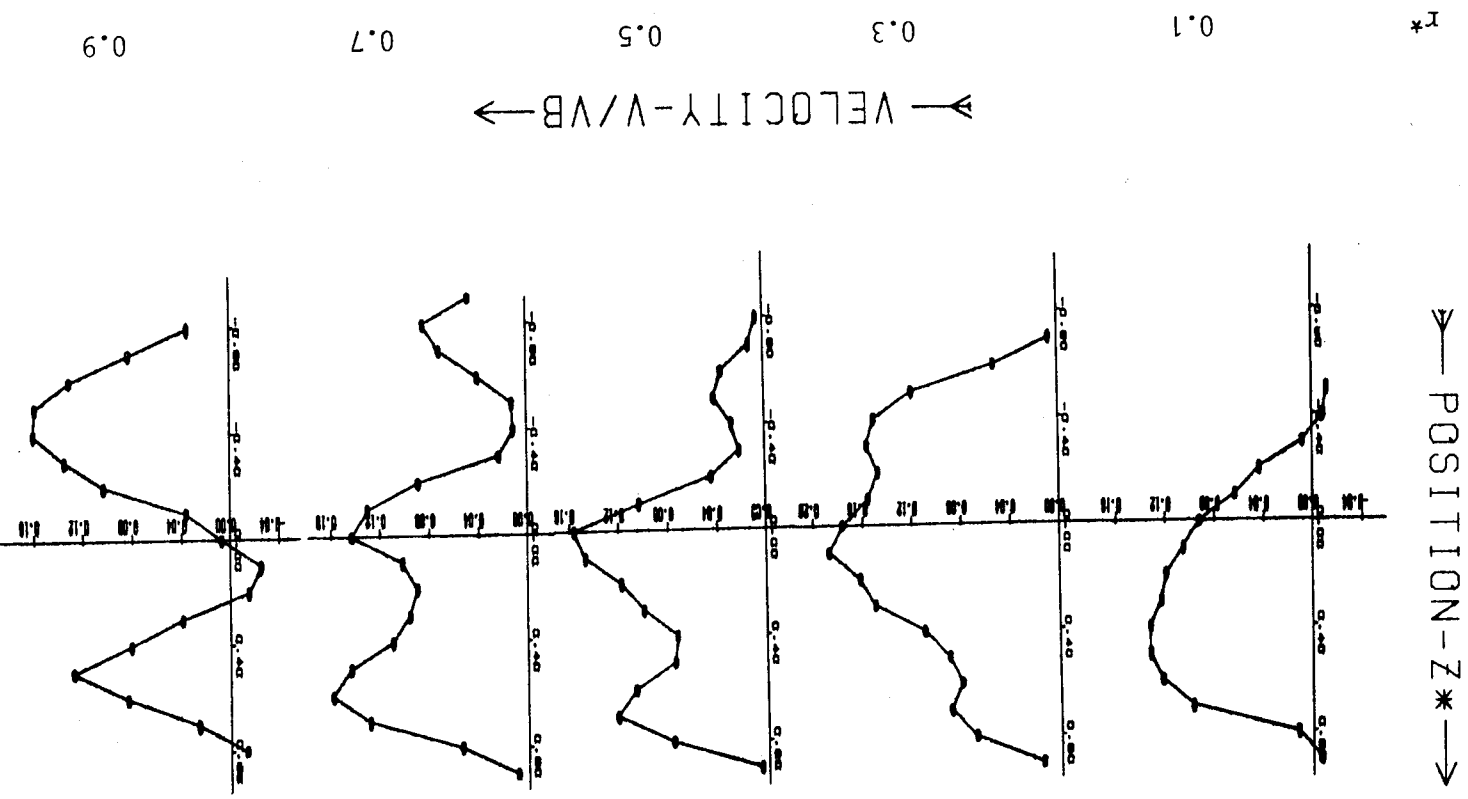
Figure 6. Rectangular diffuser, laminar flow: Profiles of V at the exit plane.

40
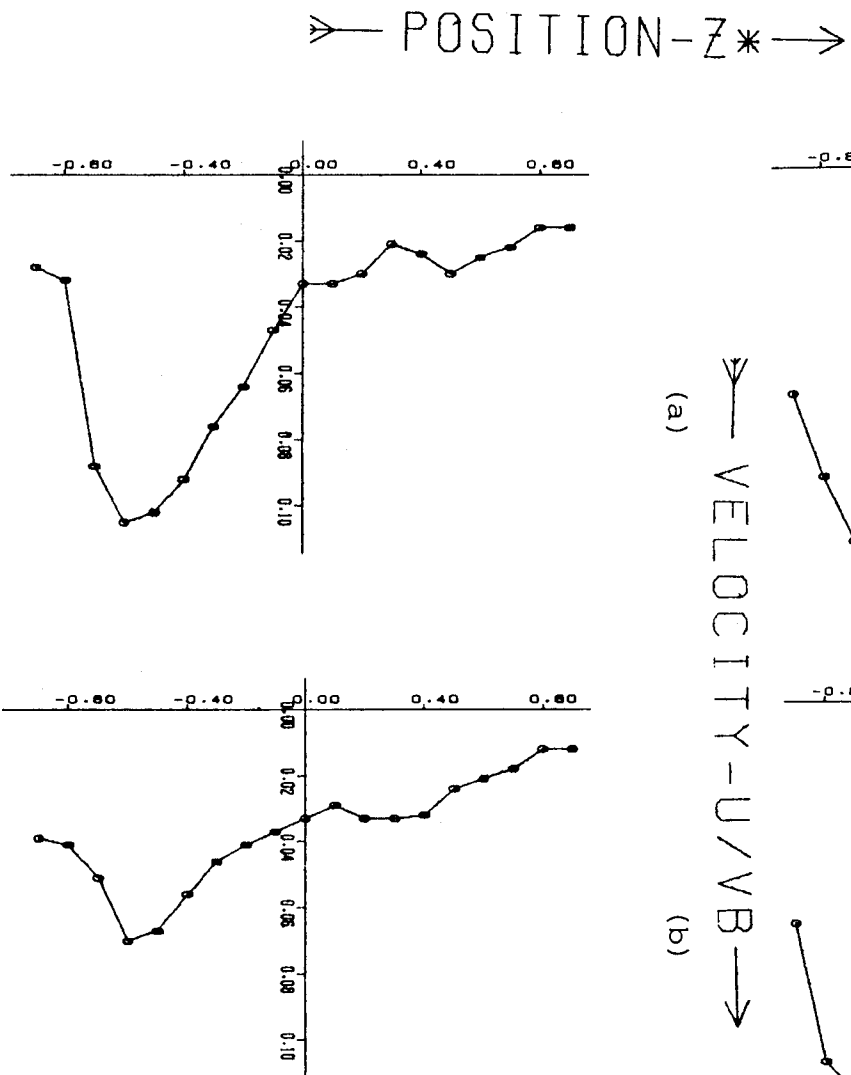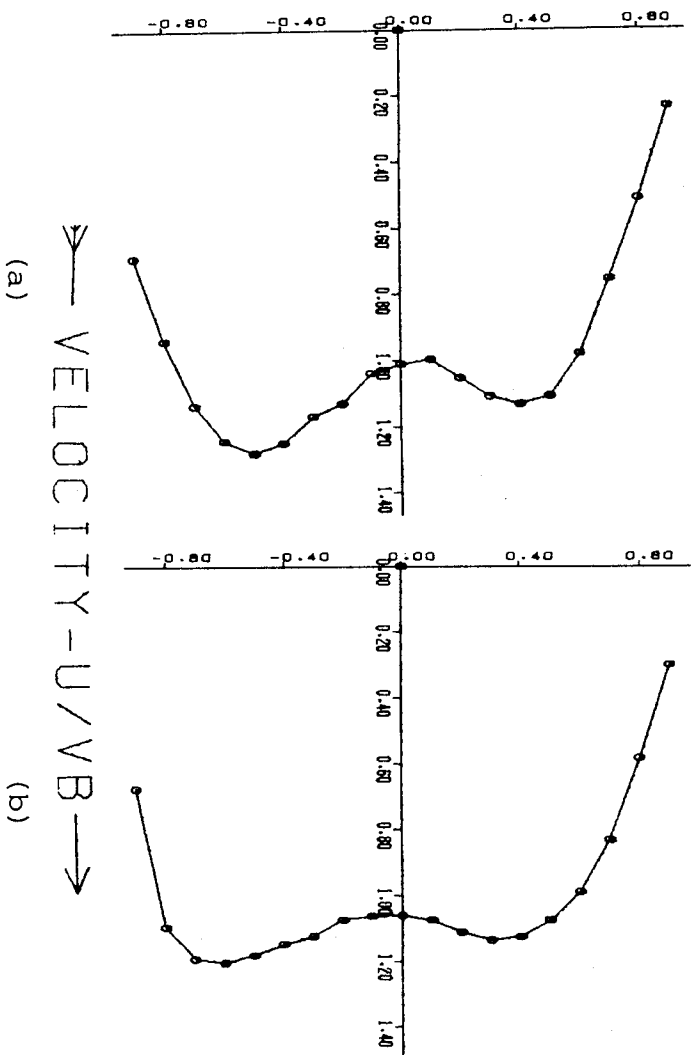
Figure 7. Rectangular duct, laminar flow:
Profiles of (a) U at X* = 12.375,
(b) U at X* = 16.735,
(c) V at X* = 12.375,
and (d) V at X* = 16.735
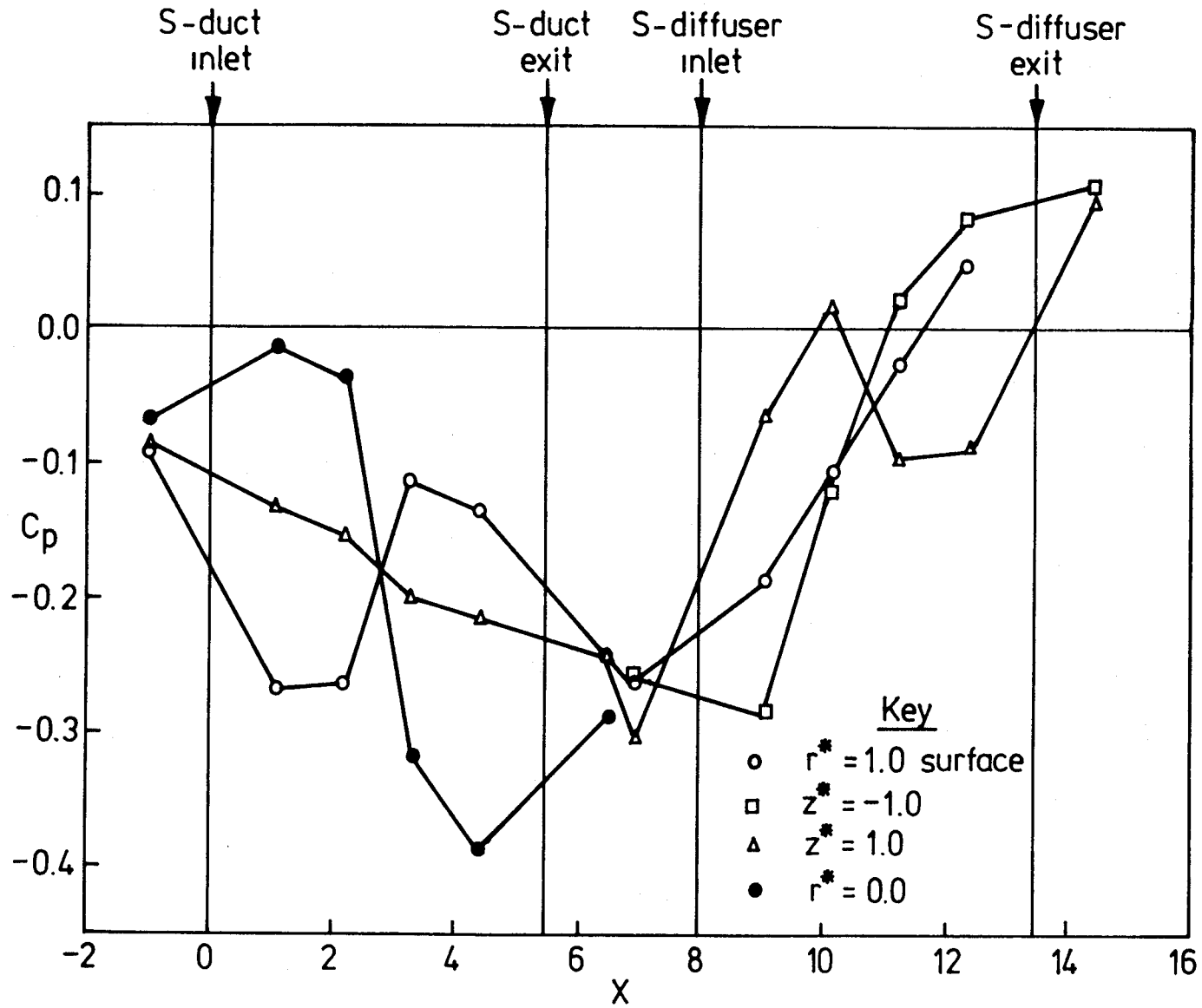
Figure 8. Rectangular duct, turbulent flow: C_p variation
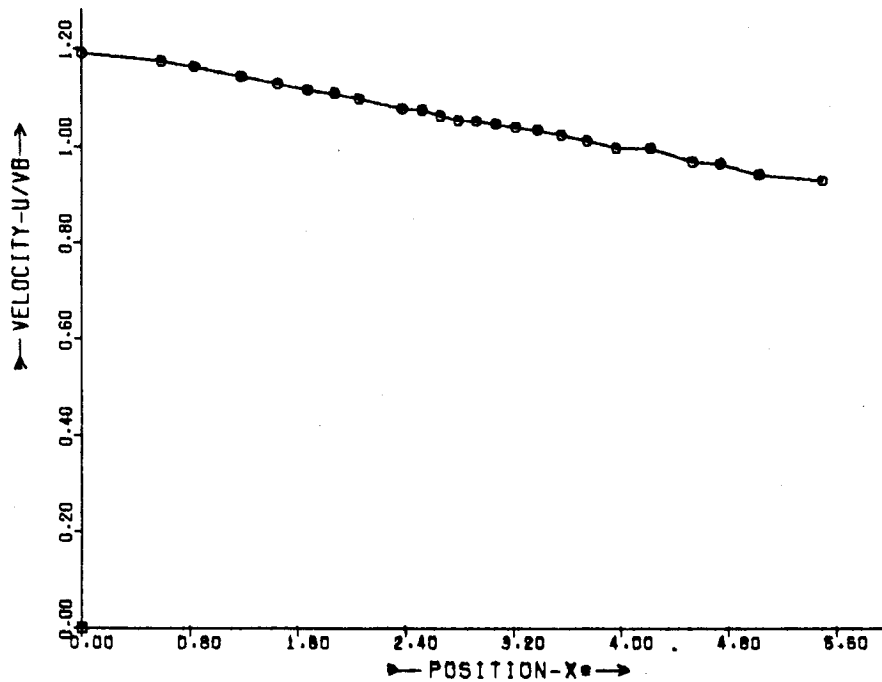
Figure 9. Rectangular diffuser, turbulent flow: Centerline variation of $\overline{U}$ velocity.
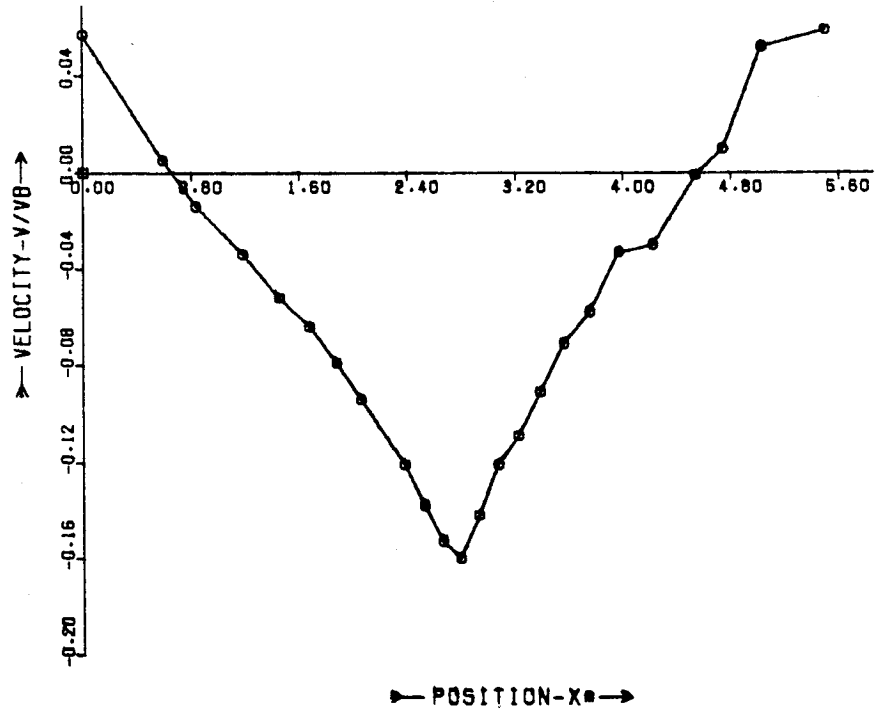
Figure 10. Rectangular diffuser, turbulent flow: Centerline variation of $\overline{V}$ velocity
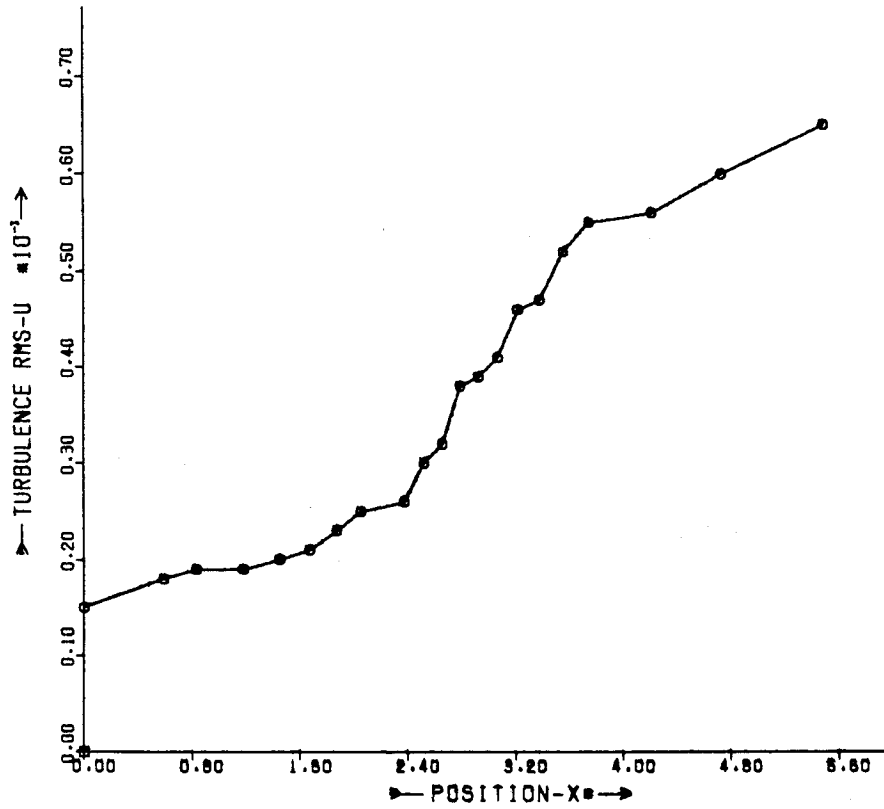
Figure 11.   Rectangular diffuser turbulent flow:
Centerline variation of $\tilde{u}$
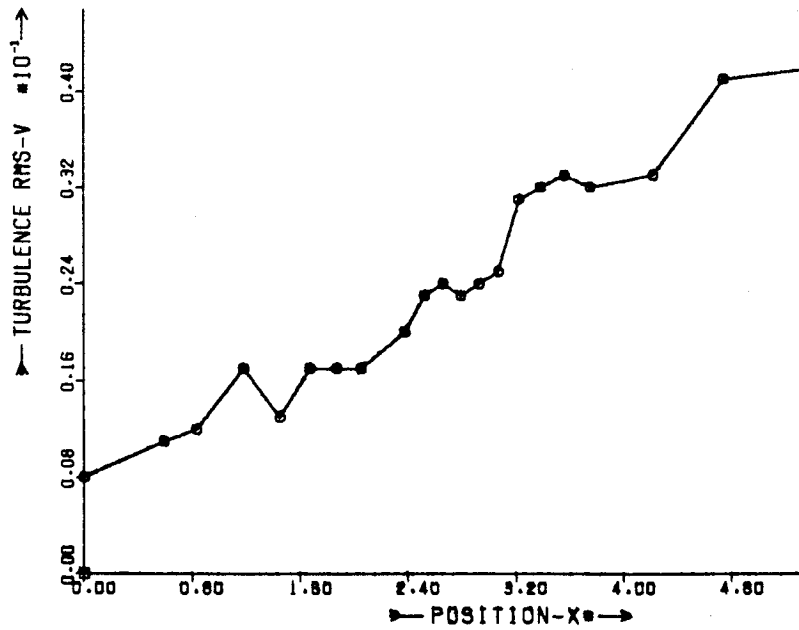
Figure 12.   Rectangular diffuser, turbulent flow:
Centerline variation of $\tilde{v}$
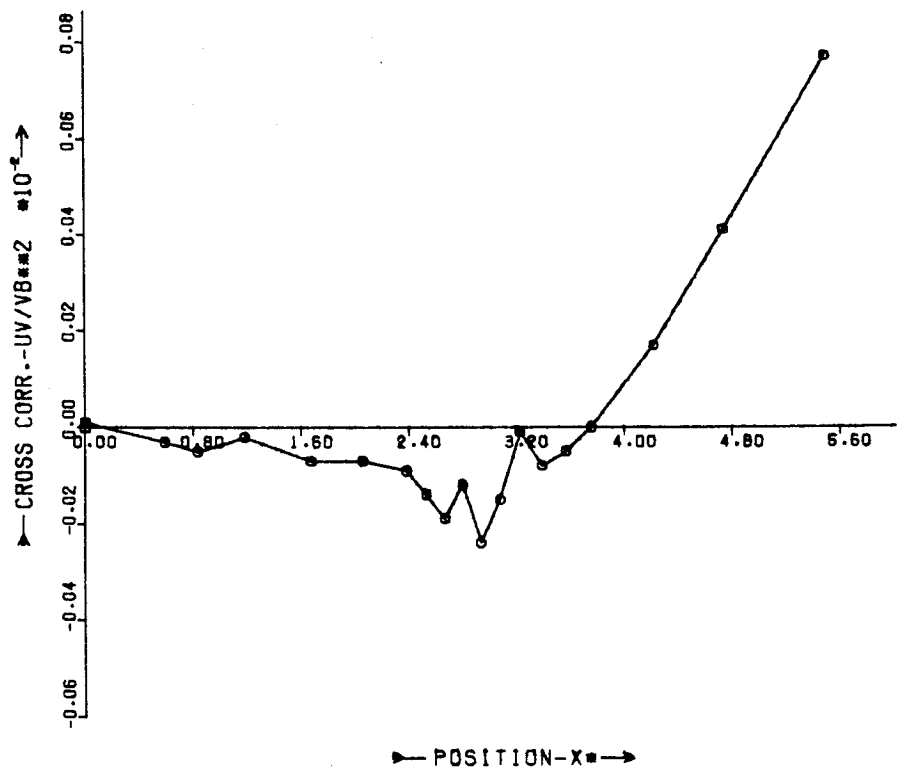
Figure 13. Rectangular diffuser, turbulent flow:
Centerline variation of $\overline{uv}$
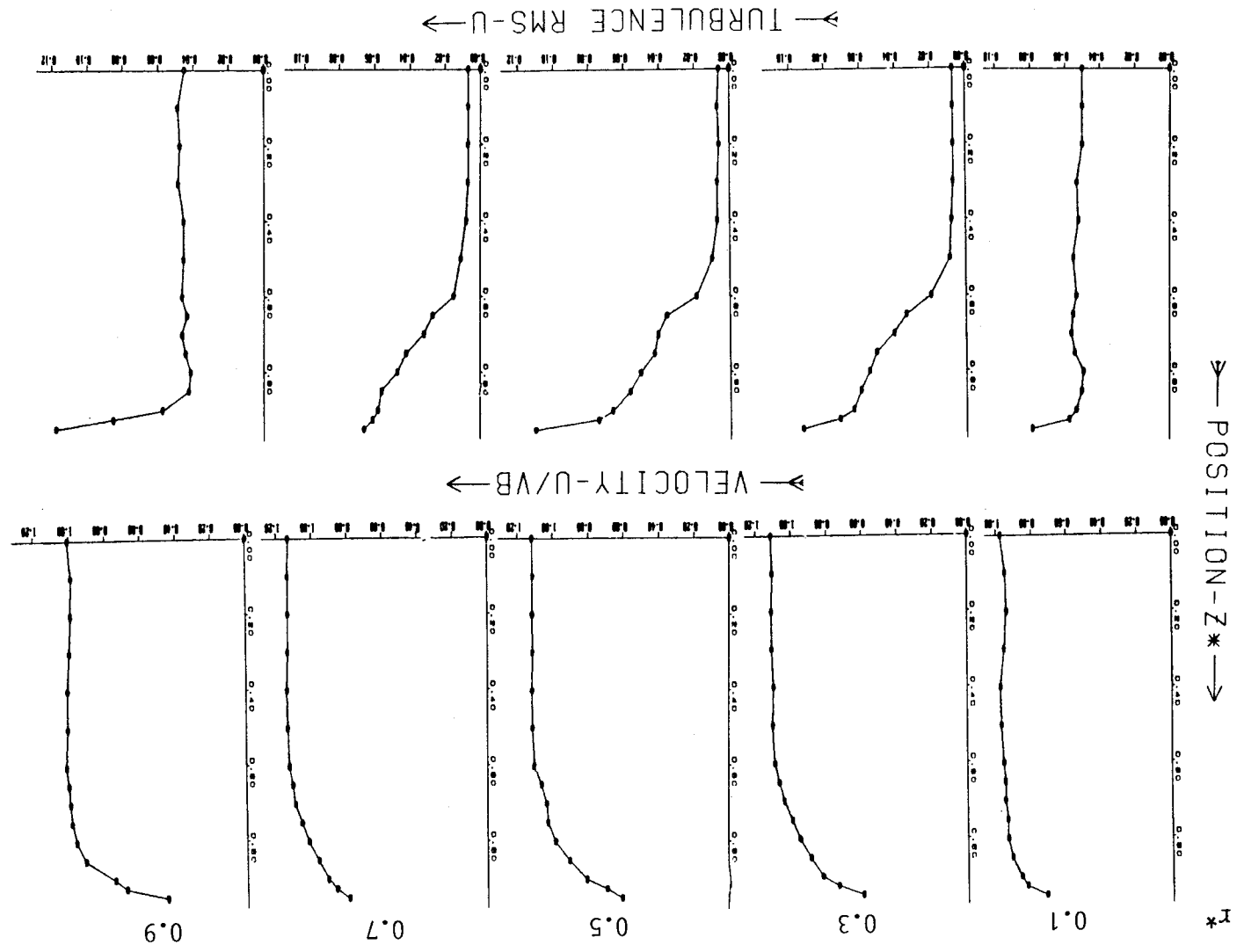
Figure 14. Rectangular duct, turbulent flow: Profiles of $\bar{U}$ and $\tilde{u}$ at the inlet plane (station 1)
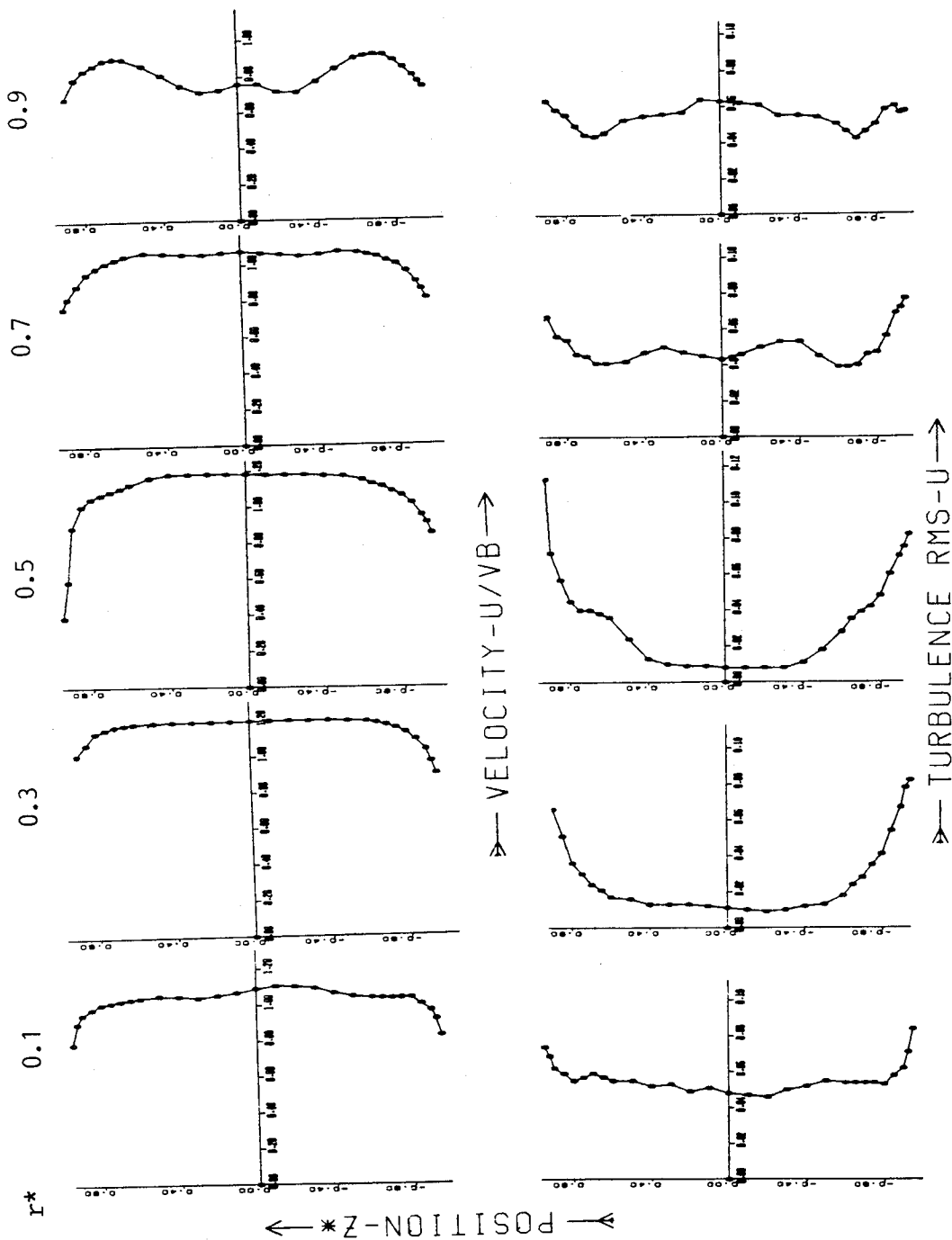
Figure 15. Rectangular duct, turbulent flow: Profiles of $\bar{U}$ nd $\tilde{U}$ at station 2.

47
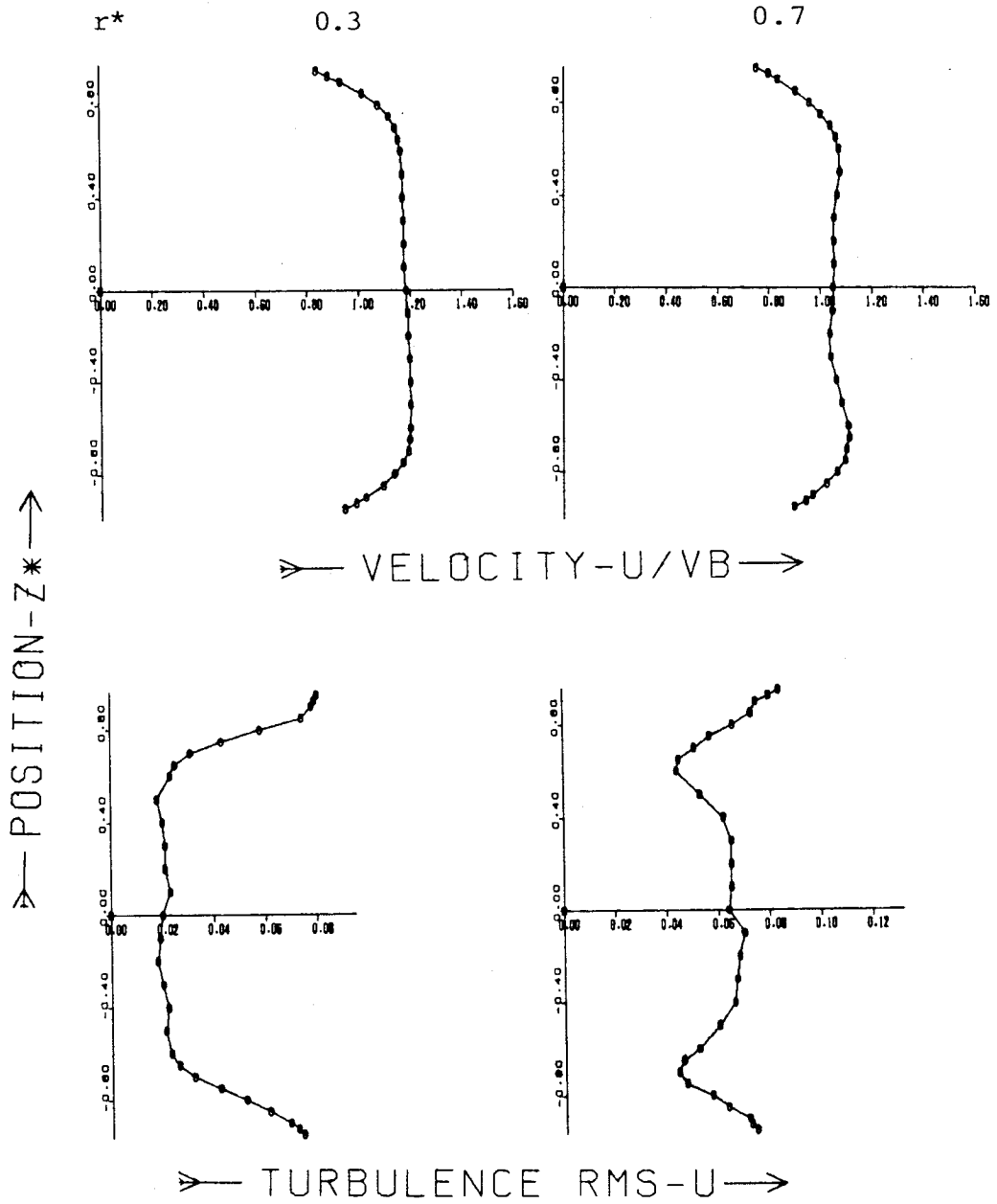
Figure 16. Rectangular duct, turbulent flow:
Profiles of $\overline{U}$ and $\tilde{u}$ at the S-diffuser inlet
(station 3)

48
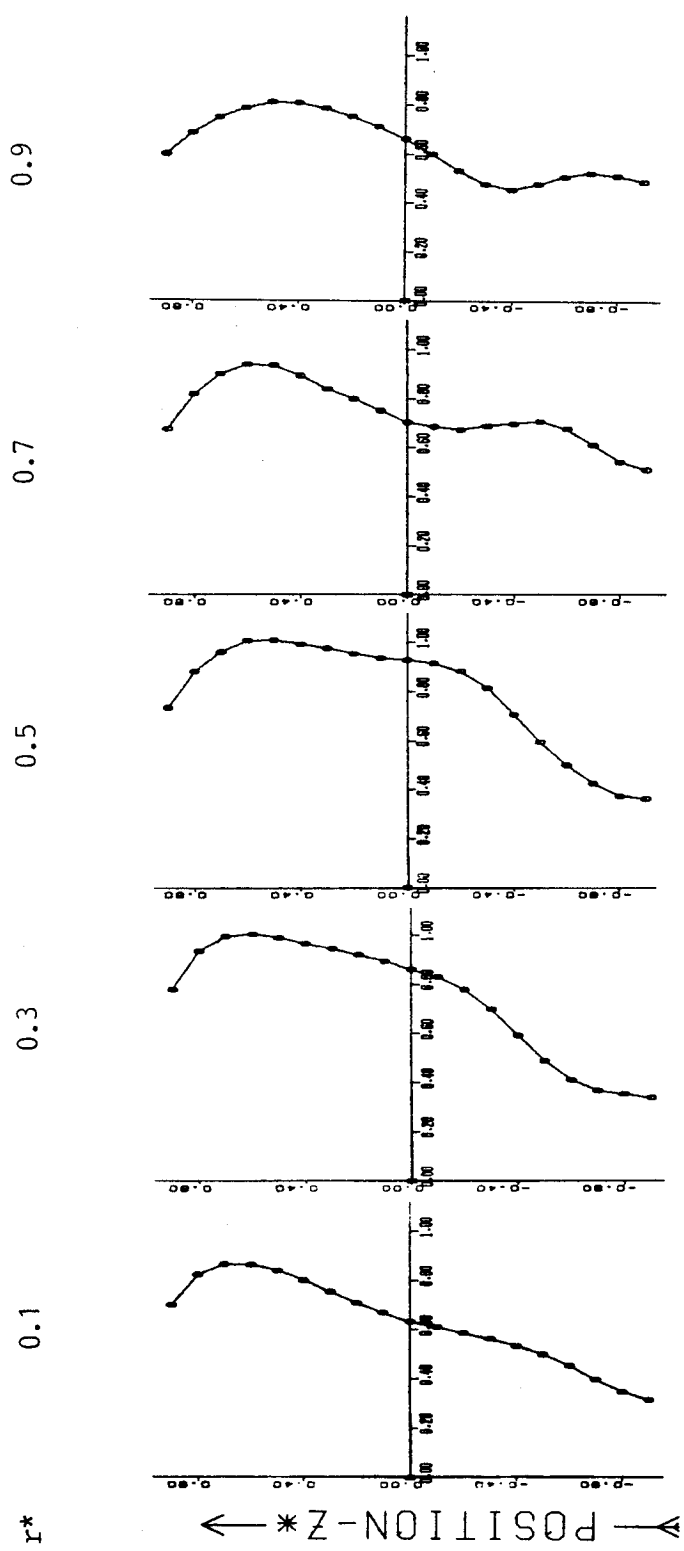
Figure 17. Rectangular duct, turbulent flow: Profiles of U at the exit of the S-diffuser (station 4)
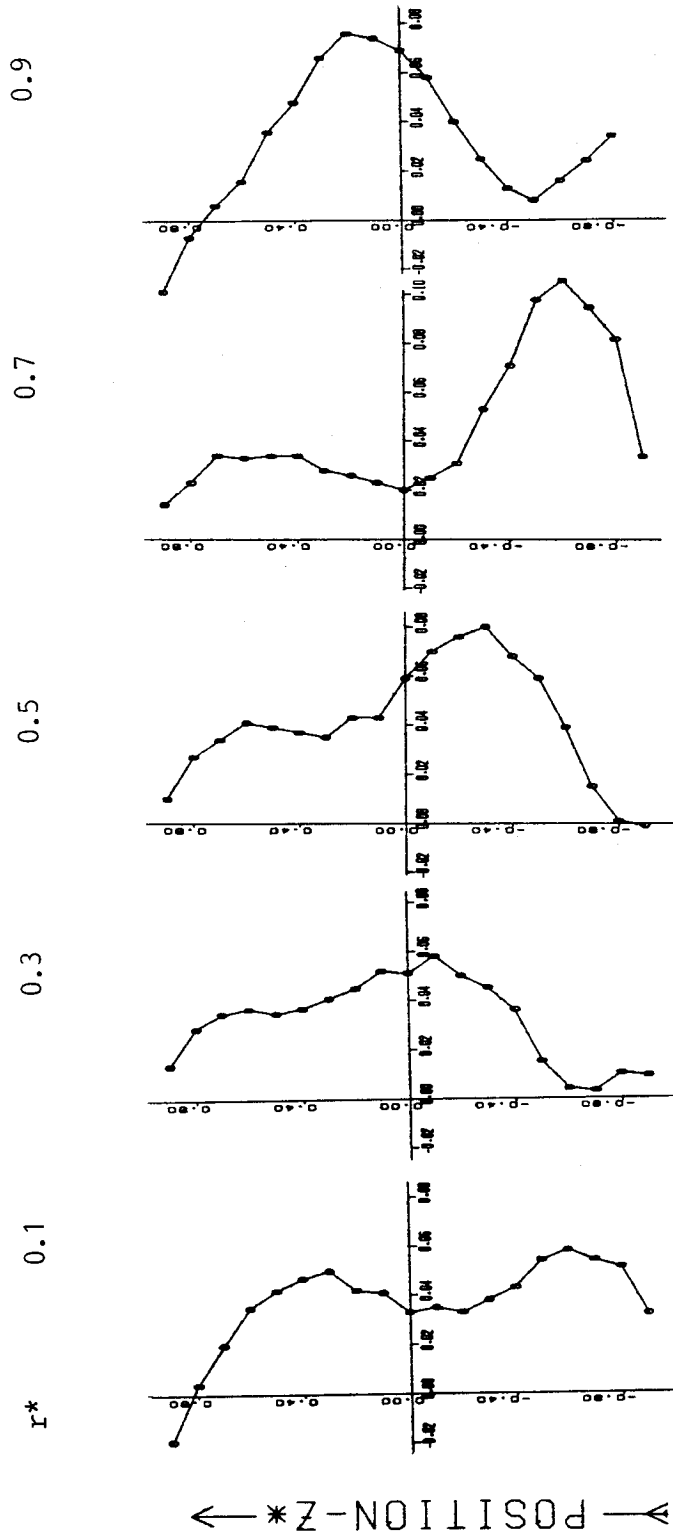
Figure 18. Rectangular duct, turbulent flow: Profiles of $\bar{V}$ at the exit plane (station 4)
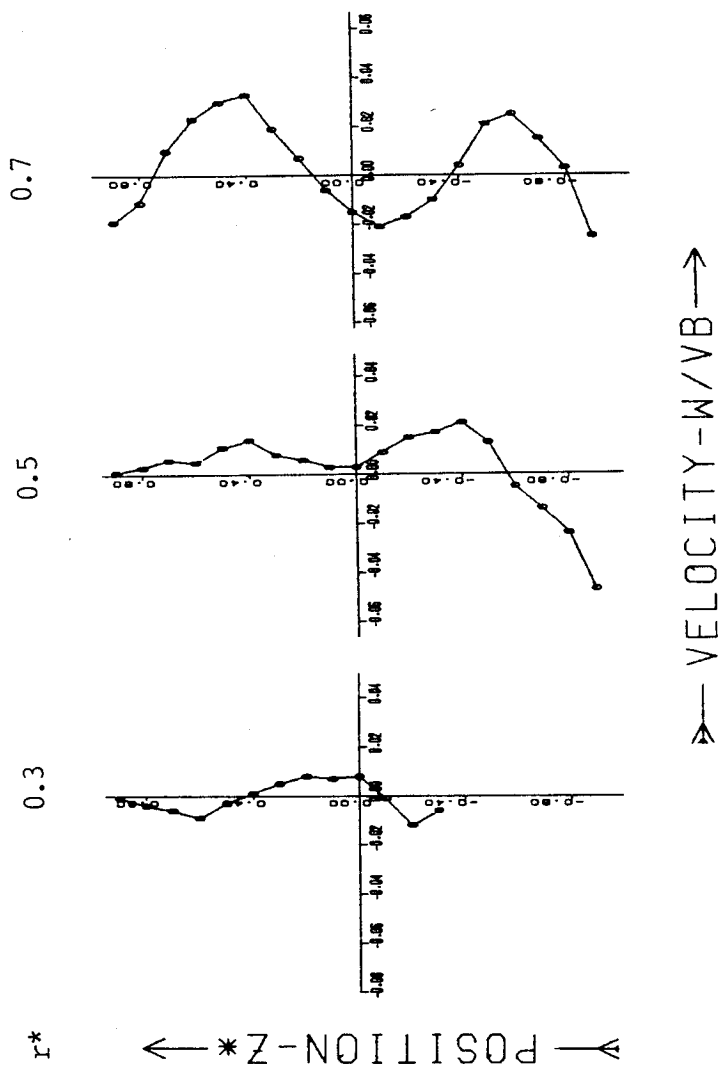
Figure 19. Rectangular duct, turbulent flow: Profiles of $\overline{W}$ at $X^* = 5.825$
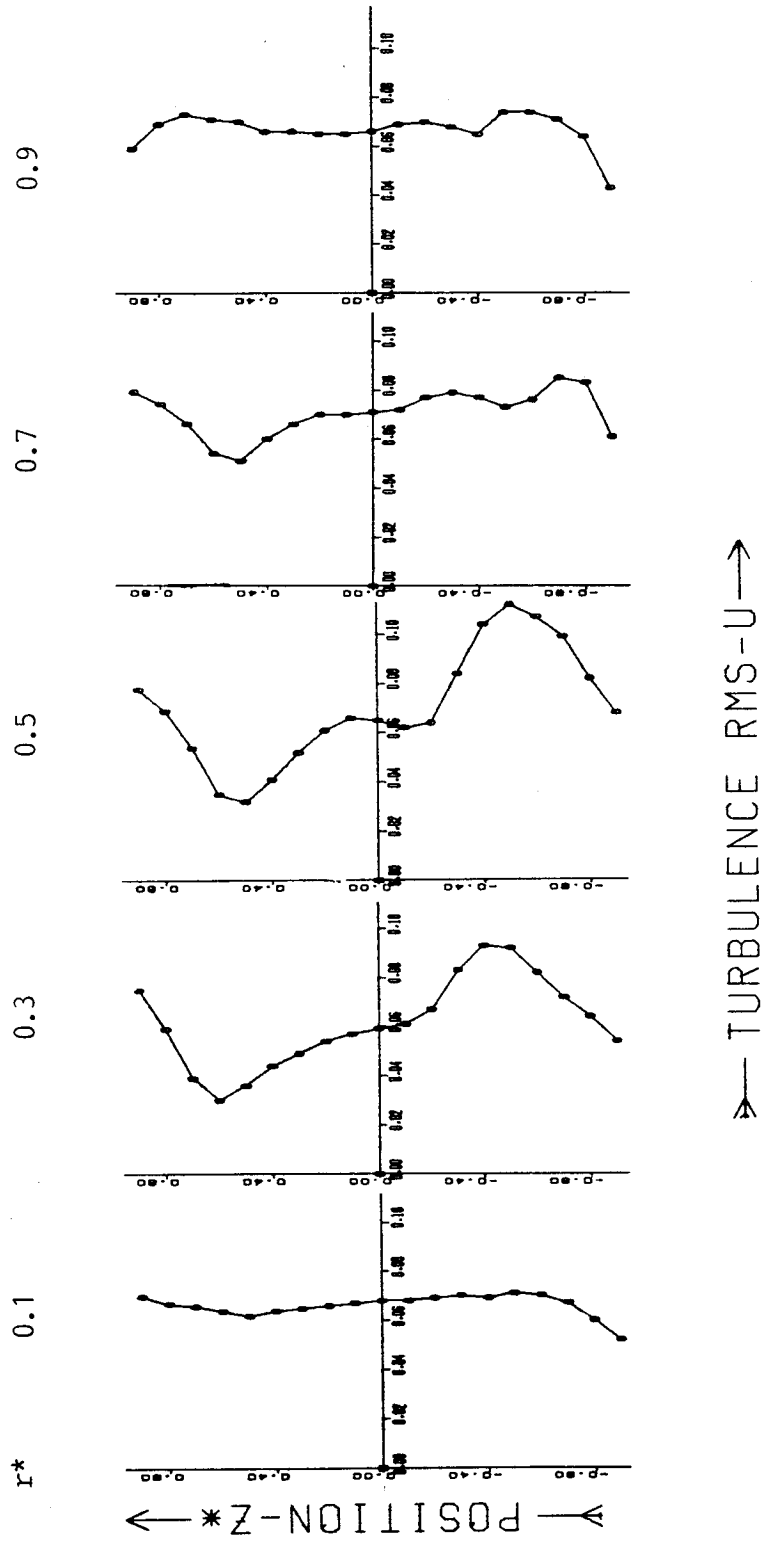
Figure 20. Rectangular duct, turbulent flow: Profiles of ũ at the S-diffuser exit (station 4)
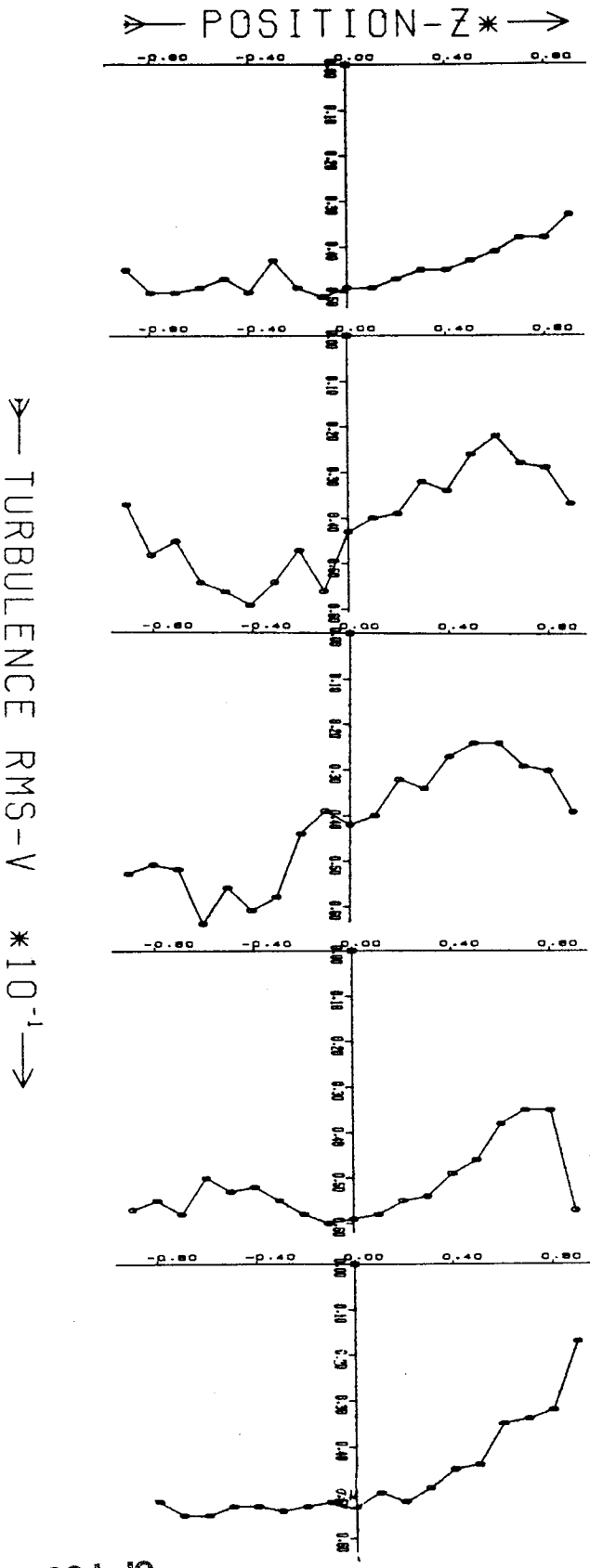
Figure 21. Rectangular duct, turbulent flow: Profiles of $\tilde{v}$ at the exit plane (station 4)

Figure 22. Rectangular duct, turbulent flow: Profiles of $\overline{uv}$ at the exit plane (station 4)

CROSS CORR.-UV/VB**2 *10⁻²

POSITION-Z*

*Y
0.9   0.7   0.5   0.3   0.1

54
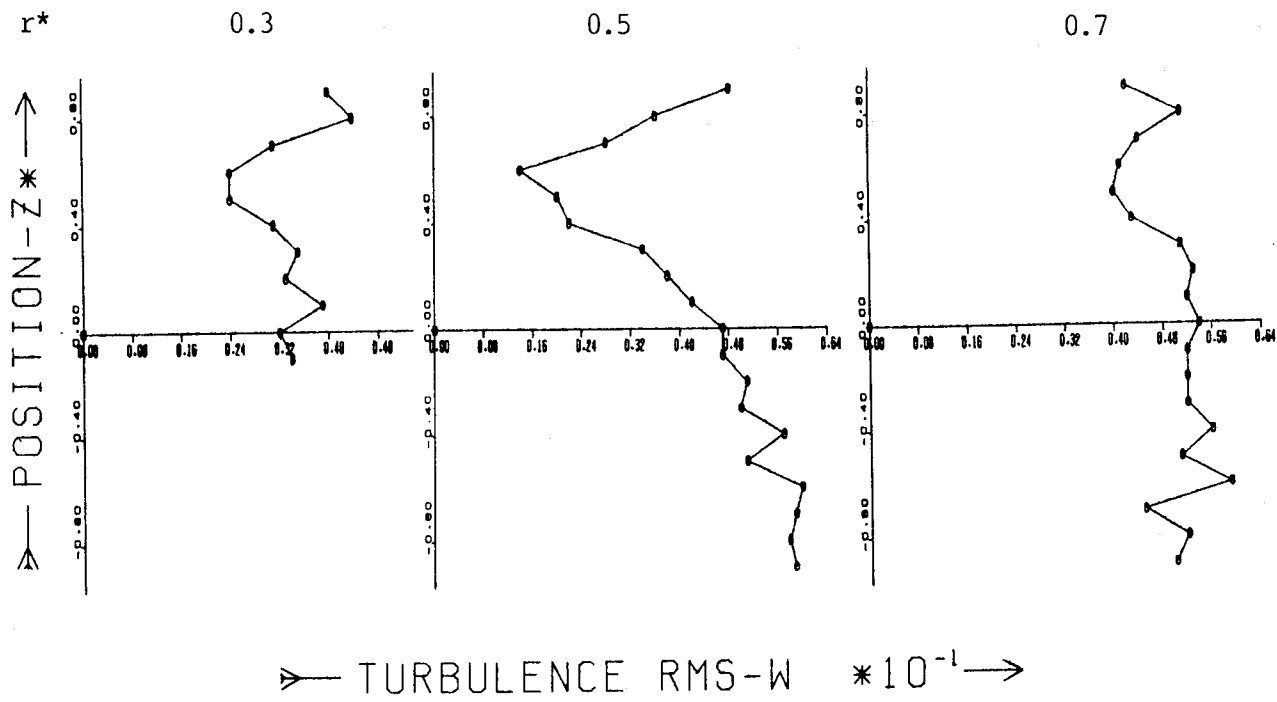
Figure 23.   Rectangular duct, turbulent flow: Profiles of $\tilde{w}$ at $X^* = 5.825$
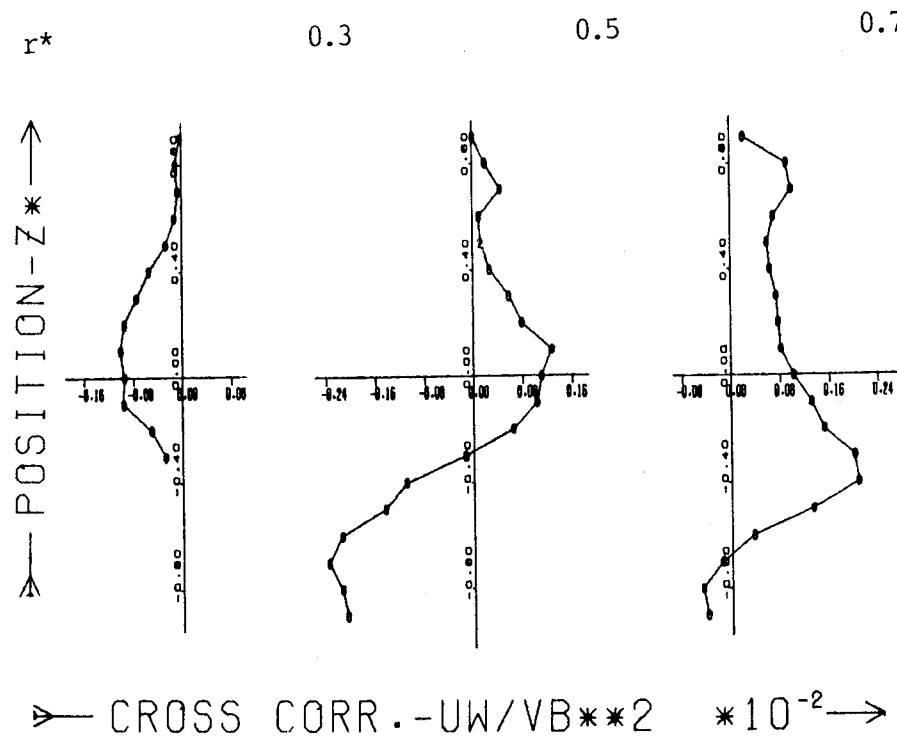
Figure 24. Rectangular duct, turbulent flow: Profiles of $\overline{uw}$ at X* = 5.825
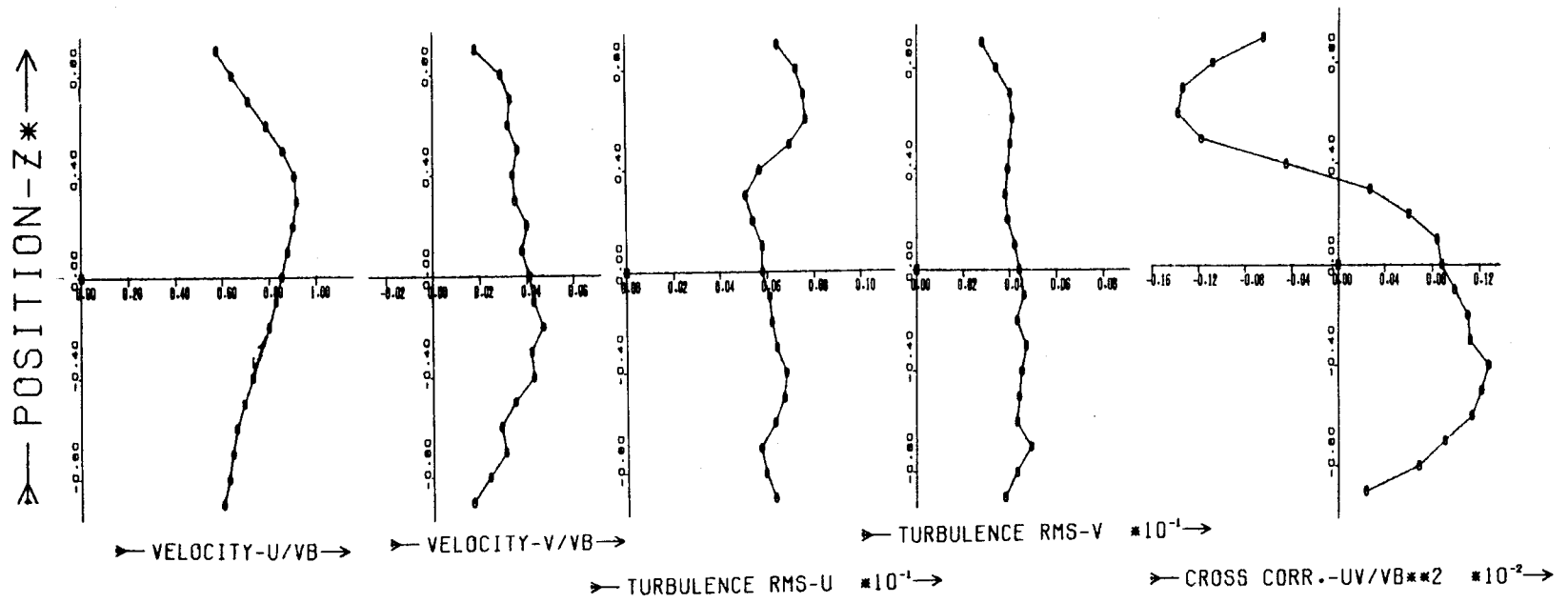
Figure 25 (a). Rectangular duct, turbulent flow: Profiles of $\overline{U}$, $\overline{V}$, $\tilde{u}$, $\tilde{v}$ and $\overline{uv}$ at X* = 12.375, r* = 0.5
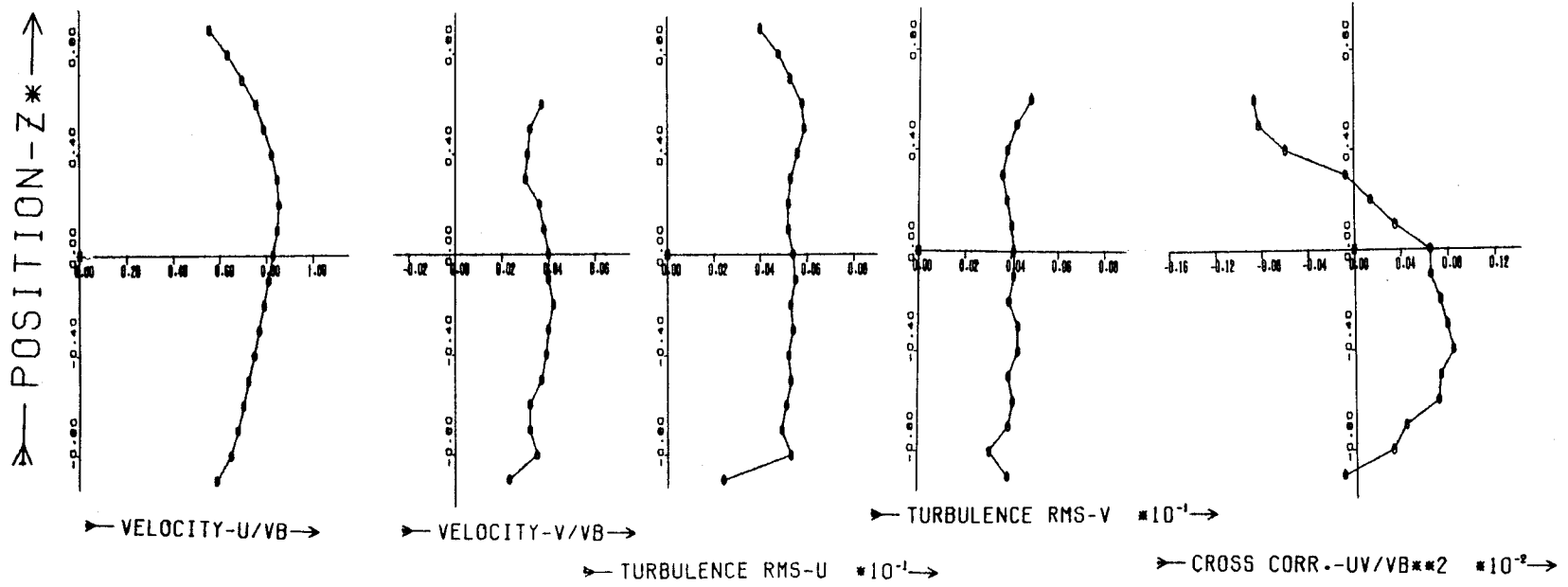
Figure 25 (b). Rectangular duct, turbulent flow: Profiles of $\bar{u}$, $\bar{V}$, $\tilde{u}$, $\tilde{v}$ and $\overline{uv}$ at $X^* = 16.735$, $r^* = 0.5$
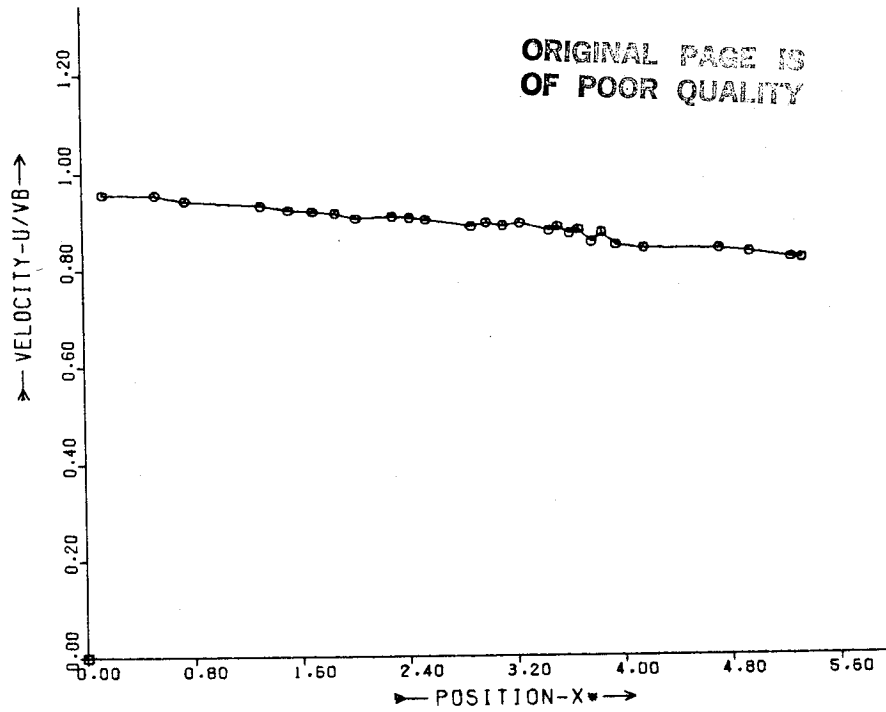
Figure 26. Circular duct: Centerline variation of $\overline{U}$
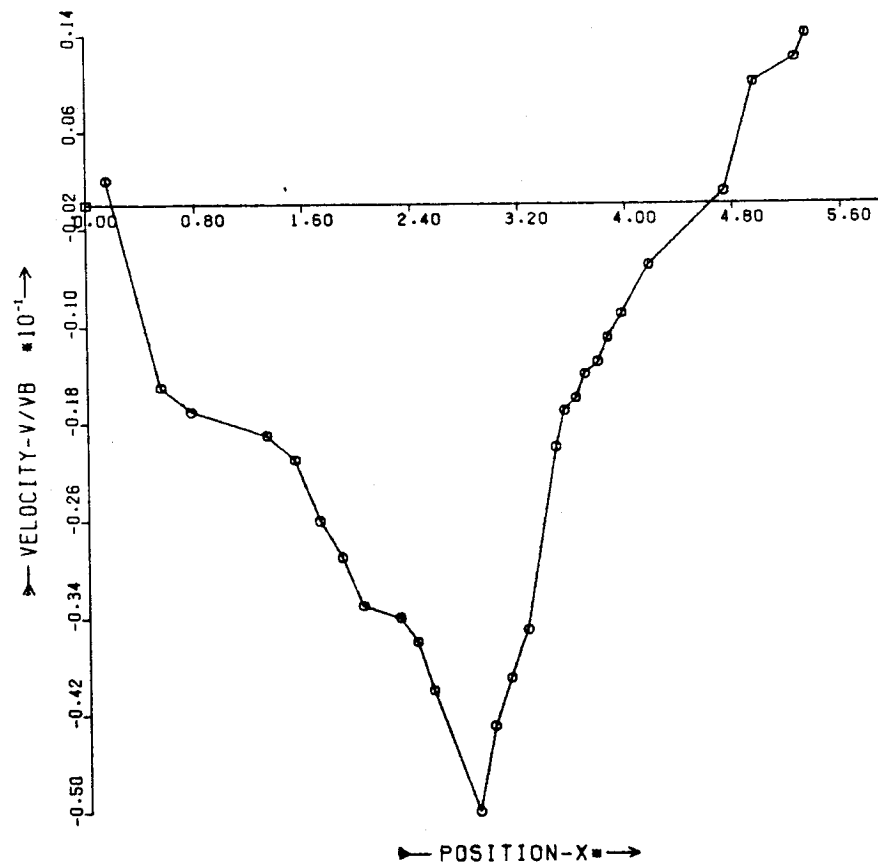
Figure 27. Circular duct: Centerline variation of $\overline{V}$

59
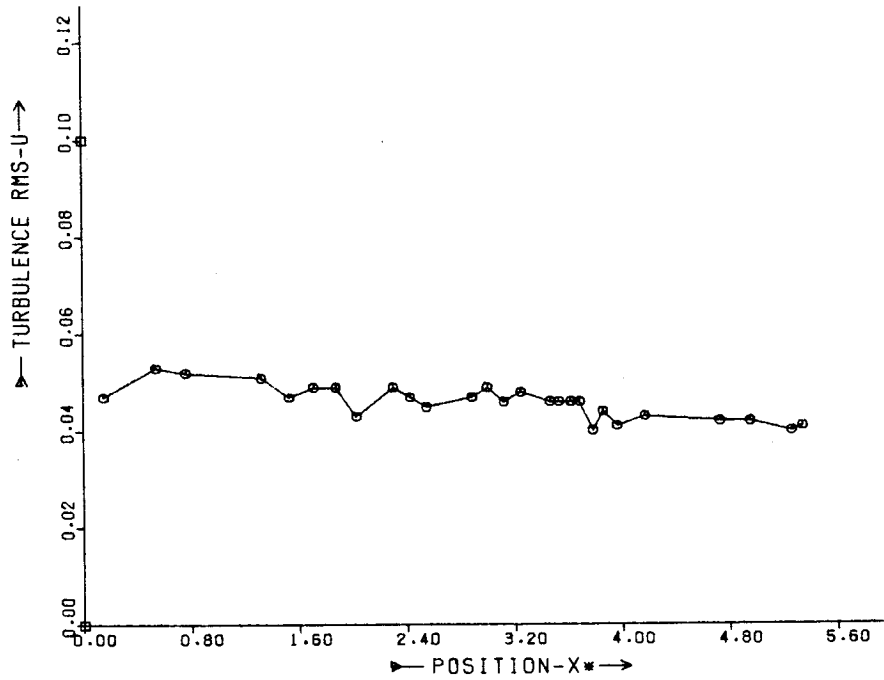
Figure 28.   Circular duct: centerline variation of $\tilde{u}$
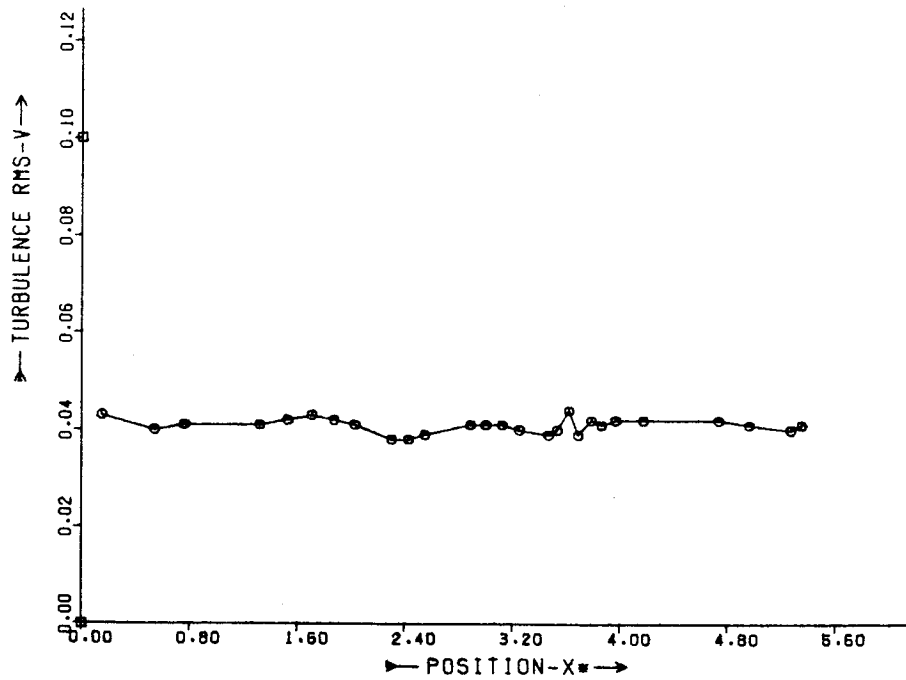
Figure 29.   Circular duct: centerline variation of $\tilde{v}$
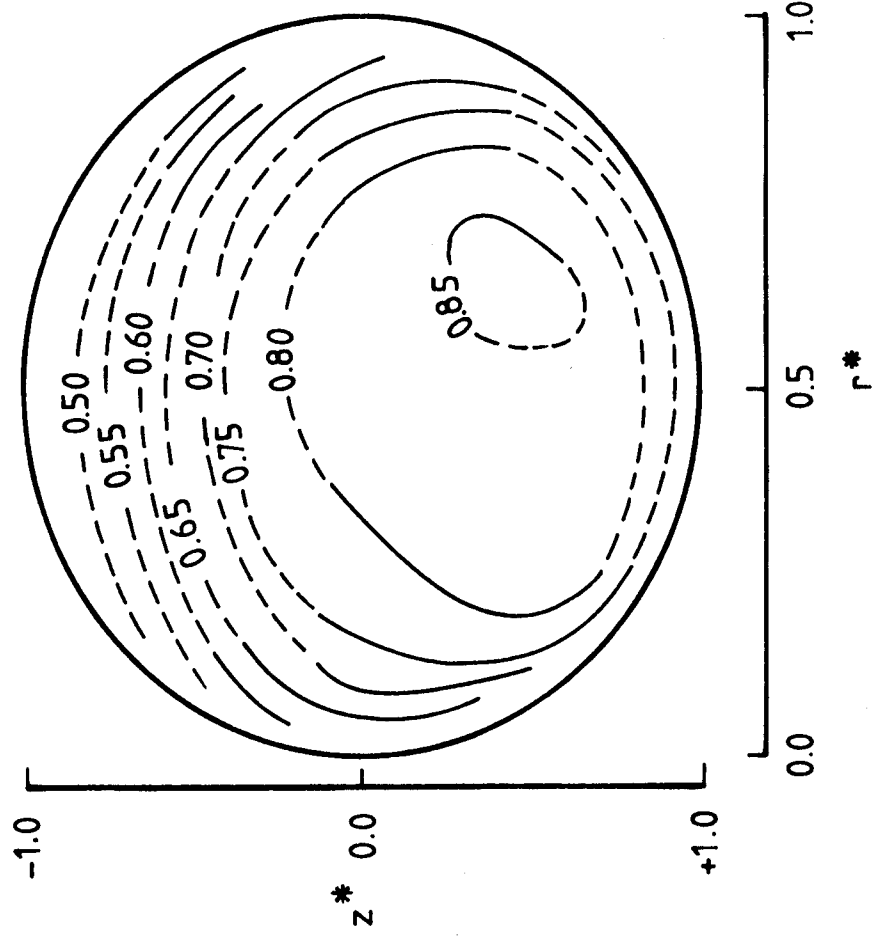
Figure 30.   Circular duct: Contours of $\overline{U}/V_B$ at the exit plane

61
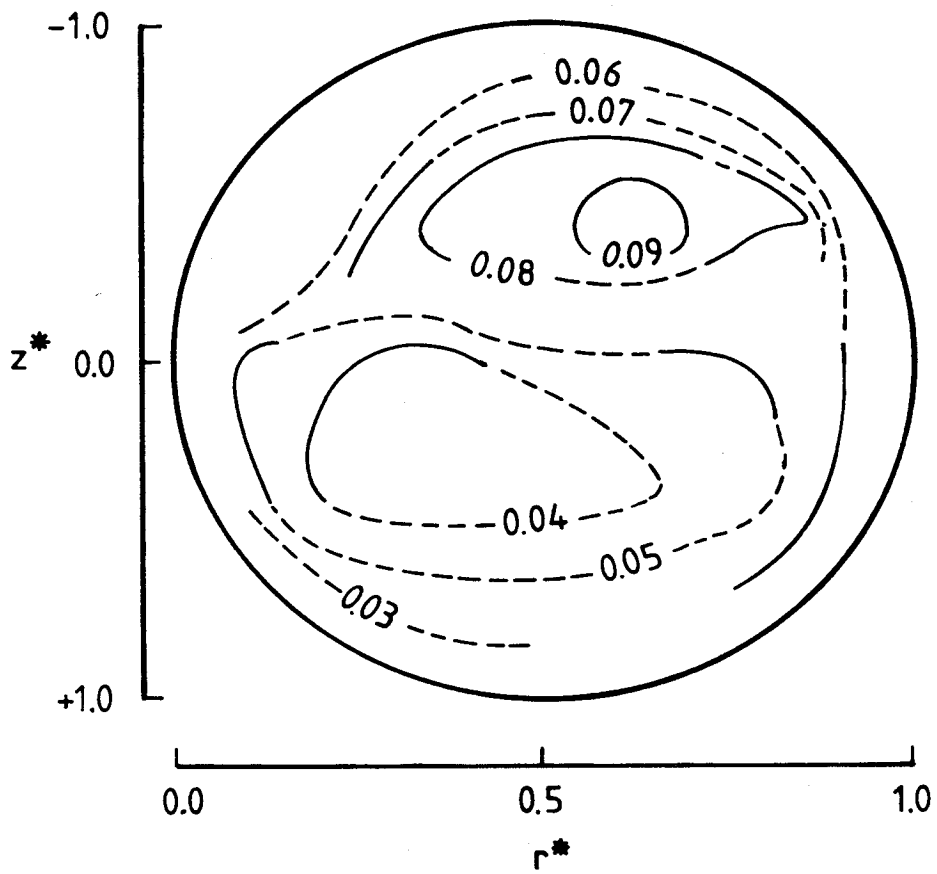
Figure 31. Circular duct: Contours of $\tilde{u}/V_B$ at the exit plane
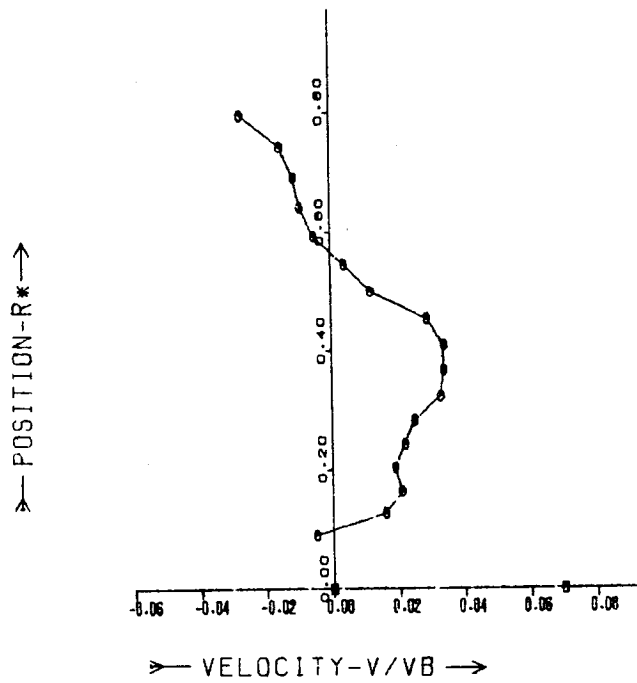
Figure 32. Circular duct: Profile of $\overline{V}$ at the exit plane, $z^* = 0.0$
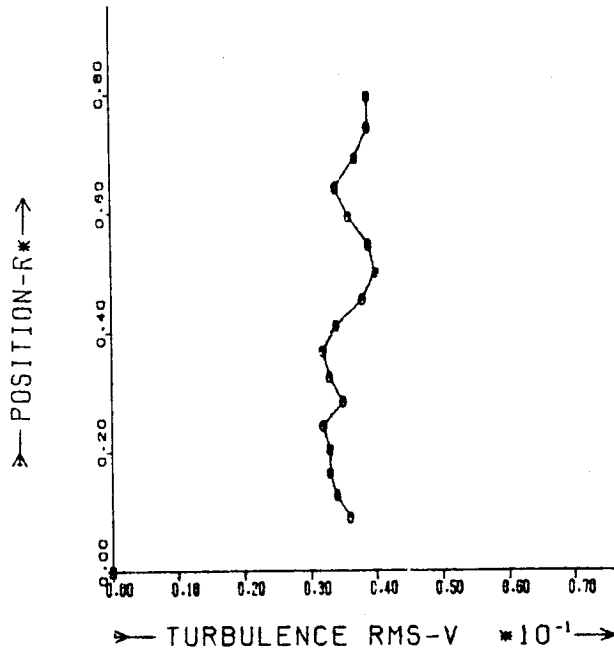

Figure 33. Circular duct: Profile of $\tilde{v}$ at the exit plane, $z^* = 0.0$
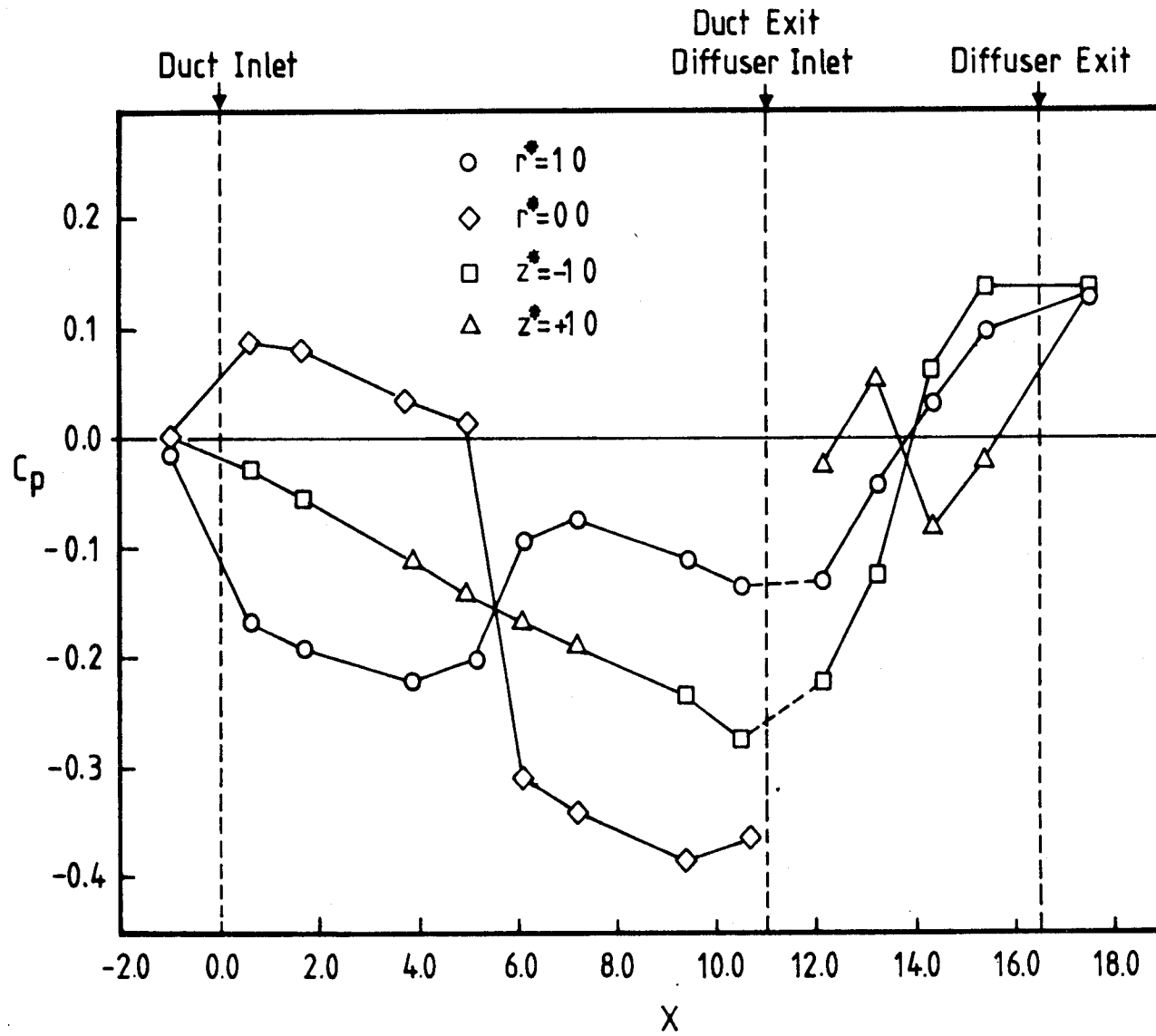
Figure 34. Circular duct: C_p variation